Deterministic Lateral Displacement Devices

-Stretching the Limits of Separation-

Jason Beech

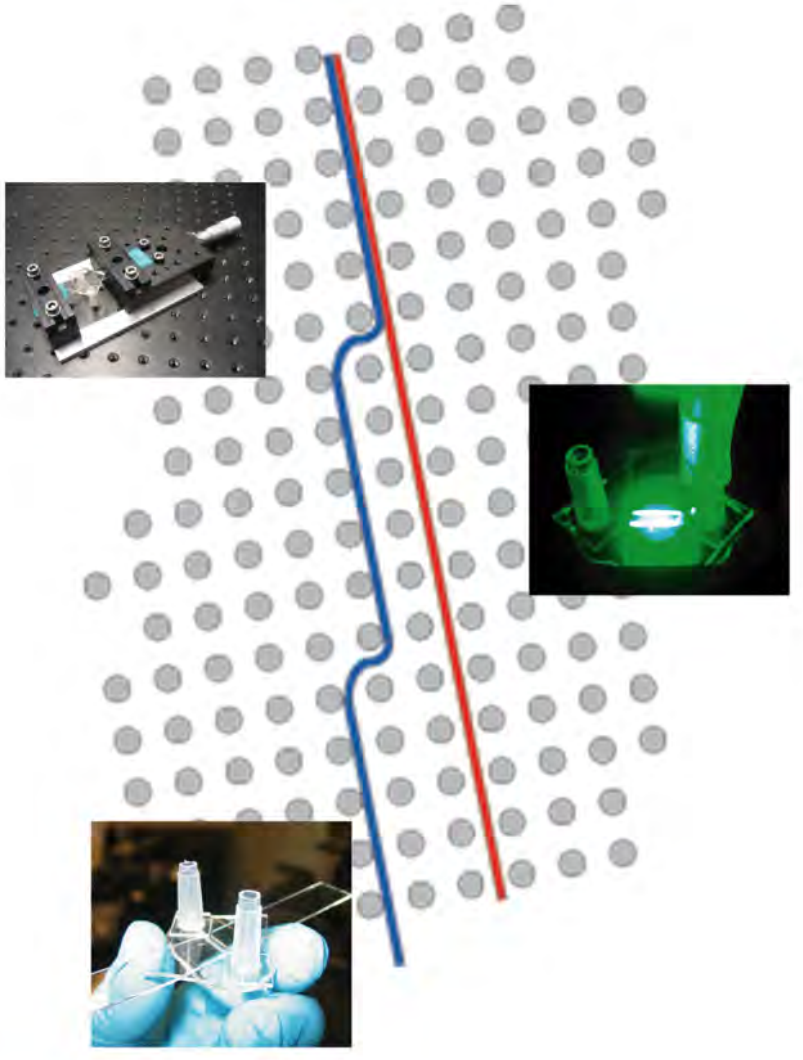

Masters Thesis *Spring 2005*

Supervisor: Jonas Tegenfeldt
Division of Solid State Physics
University of Lund

Elastic Deterministic Lateral Displacement Devices
-Stretching the Limits of Separation-

Masters Thesis

Jason Beech

Supervisor: Jonas Tegenfeldt

Spring 2005

Department of Physics
Division of Solid State Physics

LUND UNIVERSITY

Preface and Acknowledgements

This project was carried out in the period spanning from august 2004 to June 2005 at the Solid State Physics department at the University of Lund and was submitted in order to fulfill the requirements for the attainment of a MSc degree in physics.

I would like to take this opportunity to thank those people who, with their various contributions have made the completion of this project not only possible, but also an enjoyable experience.

Firstly I would like to thank my supervisor Jonas Tegenfeldt, who from my introduction to the world of experimental biophysics on one of his courses, to the inception and subsequent completion of this project has been a source not only of inspiration and support but has, with his willingness to listen to my ideas, given me confidence in my ability to pursue a career in research.

I would also like to acknowledge the contributions of Prof. Henrik Bruus and MSc. Martin Heller from the Microfluidics Theory and Simulation Group (MIFTS) at the Technical University of Denmark with whom we have collaborated on this project, for sharing their knowledge of microfluidics and the results of their simulations.

One of the reasons this project has been such an enjoyable experience is the atmosphere in the Bio Group within which the work has taken place. Thanks to all in the Bio Group, especially Richard Bunk for his help with my Mac, Rodolphe Marie and Patrik Carlberg for their many tips and practical pointers, Professor Fredrik Höök for his encouragement and Andreas, Sara, Emmanuel, Aline and Magnus for their easy going camaraderie.

Thanks also to Mariusz Graczyk, Ivan Maximov, David Adolf, Lena Timby and Bengt Bengtsson for their help with practicalities, especially Mariusz for his help with UV lithography masks.

Lastly I would like to thank my wife Nelly and my children Jonatan and Freja for not caring in the least about biophysics or particle separation or anything else that goes on here at the solid state physics department but for being happy for me as long as I'm happy doing what I enjoy. I love you.

Abstract

A new method of particle separation known as Deterministic Lateral Displacement (DLD) has been reported recently [1]. The technique separates particles continuously, by forcing them to follow varying streamlines in a laminar flow bifurcated around an array of obstacles. The range of particle sizes that can be separated in a device depends on both the orientation of the array of obstacles with respect to the flow and also on the distance between obstacles.

The elastomeric properties of PDMS can be utilised to achieve tuneable particle separation in Deterministic Lateral Displacement devices via the alteration of inter-obstacle distances.

Initial results show that the distance between obstacles can be adjusted with an uncertainty of only 90nm which confers the ability to tune the cutoff size, in the devices we fabricated, with an uncertainty of 24nm.

Glossary of Terms and Acronyms

Definitions

Aspect ratio - the ratio between depth and width of channels or features.

Coefficient of Deviation (CV) – the standard deviation expressed as a percentage of the mean value.

$$Strain(\varepsilon) = \frac{\Delta l}{l}$$

$$Stress(\sigma) = \frac{F}{A}$$

$$Poisson's\ ratio(\mu) = -\frac{\varepsilon_{\perp}}{\varepsilon_{11}}$$

Acronyms and Abbreviations

(E) DLDD - (Elastic) Deterministic Lateral Displacement Device
SAT - Suspension Array Technology
Re - Reynolds number
Pe - Peclet number
PDMS - Poly (dimethylsiloxane)
EOF - Electroosmotic flow
CE - Capillary Electrophoresis
ElFFF-Electric Field Flow Fractionation
SdFFF-Sedimentation Field Flow Fractionation
ThFFF-Thermal Field Flow Fractionation
FlFFF-Flow Field Flow Fractionation
SDS-PAGE – Sodium dodecylsulphate-polyacrylamide

List of Figures

List of Tables

Contents

Chapter 1

Introduction

The separation of particles by size is integral to many of the analytical and preparative techniques used in the fields of medicine and biology. Recently a Deterministic Lateral Displacement Device (DLDD) has been reported in the literature [1]. The device, based on the bifurcation of flow around obstacles in a microchannel is able to resolve a 1 percent difference in particle size in the micrometer range in under 1 minute. The DLDD differs from conventional methods of particle separation, such as gel electrophoresis, field-flow fractionation and size exclusion chromatography in its non-dependence on stochastic mechanisms. Unlike the later, the DLDD can be run at arbitrarily high speeds, the result being an increase in resolution and faster separation times.

The obvious direction for the future development of the DLDD is the scaling down of structures and the subsequent decreasing of the particle sizes that the devices can separate, proteins, peptides and viruses to name a few examples. A recent article in the Industrial Physicist [2] stresses the need for new technologies that would, "…improve our ability to separate and analyze assemblies of proteins with high speed and resolution". Eventually the traditional methods of two dimensional gel electrophoresis (2-DE) and protein arrays are likely to be replaced, but would in the meantime benefit greatly from improvements in the methods of pre-concentration and pre-treatment needed for resolution of low-abundance proteins, not least because they often signify the onset of disease or dysfunction [3].

One approach to protein analysis utilizes suspension array technology (SAT) [4]. Microspheres with distinct optical properties are used as solid supports in the same way as the spots on flat-surface microarrays, the difference being that it is the optical properties of the beads rather than the physical location on the surface that is used to distinguish the individual proteins. Tegenfeldt et al [5] have proposed the use of the DLDD´s ability to

detect small changes in size with high resolution to analyze suspension arrays. The increase in the sizes of functionalized beads due to the binding of proteins on their surfaces is on the order of 1-100nm, which is within the proven capabilities of the DLDD. Creating a device however in which the critical size is determined with an error less than 1-100nm is difficult and even when this is possible, different device geometries would be needed to obtain separation at each of the many critical sizes needed in order to analyze any meaningful fraction of the 10 000 or so proteins present in biological samples. Devices in which the critical size could be altered would be of considerable benefit. Techniques for the fractionation of DNA have been reported [6, 7] in which some degree of tuneability is possible but, these methods work only for long molecules such as DNA and not for spherical, or near-spherical, particles.

We envision two ways of altering the critical size in order to achieve tuneable separation.

The size at which separation occurs in a DLDD is dependent on two parameters, the angle between the direction of flow and the rows of obstacles, and the distance between these obstacles.

By using two perpendicular electric fields it is possible to control the direction of flow (or particle transport) [8]. This would enable control over the angle between flow and obstacle orientation. We also realised that adjusting the distance between posts could be achieved by fabricating DLDD´s in an elastic material and simply stretching or compressing them. We will call this device the elastic-DLDD or E-DLDD.

The primary aim of this project is a "proof of principle" for the E-DLDD. We aim to show that adjustment on the nanometre scale of the inter-post distance can be achieved through the mechanical deformation, on the macro-scale, of DLDD´s fabricated in PDMS rubber. The ability to tune the critical size can in its simplest application be used to move the point at which separation of a distribution of sizes into two broad bands occurs but can also be used, in other modes, to target and separate specific particle sizes from populations with large deviations in size. This and various other possible applications of the DLDD are also explored in this thesis.

1.1 Project Layout

We begin, in time honoured fashion, with a brief introduction to some of the theory one needs to grasp in order to understand how separation is achieved in the DLDD.

The DLDD is in its present form, prior to any down scaling efforts, a microfluidic device. We will introduce the reader to the field of microfluidics and describe some of the transport mechanisms important to the field of particle separation. We will look at the induction of flow in microchannels and the characteristics of the flow generated by the different methods. The respective advantages and disadvantages of each method will be considered. Band broadening due to diffusion and its effect on resolution and separating power will also be discussed.

The basic principles, applications and limitations of the more common methods of particle separation will be covered briefly before looking at the theory of the deterministic lateral displacement device itself. We try to remain conscious of the limitations of our technique and with this in mind calculate first order approximations of both the theoretical limits of

the E-DLDD and the restraints placed upon us by for example fabrication processes, material properties, bead sizes, pumps and optical detection.

It should be stressed that this is in the main part an experimental project. The fields of fluidics and separation science are extremely well developed and the introduction given here is cursory and very much simplified.

The final chapters are devoted to design and fabrication, experimental work, results and a discussion of a few of the possible applications of the E-DLDD.

Chapter 2

Transport Mechanisms

The following introduction is adapted in the most part from "Unified Separation Science" [9] by J Calvin Giddings, although other texts are also referred to.

In order for a separation to occur, it is necessary to have a transport of the molecules or particles being separated. Transport mechanisms can be divided into two main groups, transport relative to the solute or carrier medium and transport with the medium. Transport relative to the carrier medium is a selective process dependent on the forces exerted on particles, forces that in turn depend on particle properties such as size, electric charge or chemical affinity. Transport with the medium is called either bulk transport or fluid flow. It is these forces and flow mechanisms, carefully combined in a wide variety of arrangements that lead to separation in the plethora of devices that are currently used. We will concern ourselves here primarily with flow, being as it is the bifurcation of flow around posts in a microfluidics channel and the subsequent size dependent selection of migration path through a post array that leads to separation in the DLDD.

Pumps were used to induce fluid flow in the DLDD´s and we look therefore at the characteristics of flow when induced by a pressure difference. With a mind to scaling down the DLDD we consider electrokinetics, both electroosmotic flow and the electrophoretic transport of charged particles as alternatives to pressure driven flow. The difference in the characteristic flow profiles of the different methods of flow induction will have an effect on the critical size in the DLDD.

We refer the reader interested in other methods of flow induction to ref [9].

As it is diffusion that often sets the limits to the resolution of separation we shall also look at those physical properties that determine the rate of diffusion and how one can quantify its effects.

2.1 Flow

One can imagine breaking up a fluid body into a series of small elements. Each of these elements will be subject to a range of forces and will move accordingly, in the same way that a mechanical body responds to the sum of forces upon it. A fluid element will accelerate in the direction of any net force and continue at constant velocity in its absence.

Examples of the forces that act on fluid elements are pressure forces, viscous forces, gravitational forces and the centripetal forces present in centrifugation. Pressure forces originate in a pressure gradient. Sucking on a straw for example creates a pressure gradient over the length of the straw. Fluid elements will have a higher pressure on one side than the other leading to a net force and therefore all fluid elements will accelerate in the direction of lower pressure, that is, into your mouth. Viscous forces occur as fluid elements slide past one another. Viscous forces are the reason that it becomes increasing harder to suck drinks through a straw the thicker or more viscous they become. Friction forces between the fluid and the walls of the channel act also to slow flow, you cannot drink through a capillary tube, as the lungs cannot generate the force needed to overcome the friction. Gravitation leads to convection in large bodies of water and is one of the forces you compete with when drinking through a straw, but at the micrometer scale, it can often be neglected. Centripetal forces, although important in the field of separation, will not be considered here other than to mention that it could be possible to drive particles through a DLDD by mounting it in a centrifuge [10, 11].

It is possible to formulate equations of motion for a fluid in the same way one can formulate Newtonian equations for mechanical bodies. The resulting differential equation is called the Navier-Stokes equation and is basically Newton's second law for fluids [12]:

$$m \cdot a = \sum_i F_i \Leftrightarrow \rho \cdot \left(\frac{\partial u}{\partial t} + u \cdot \nabla u \right) = -\nabla P + \rho \cdot \nu \nabla^2 u + F$$

$\nu \equiv \frac{\eta}{\rho}$; is the kinematic viscosity

ρ = density

u = velocity

P = pressure

The solution of the Navier-Stokes equation gives the trajectories and velocities of all fluid elements.

The Navier-Stokes equation is a many body equation and as such cannot be solved except for in the case of steady low-velocity flow and high symmetry in the channels containing the fluid. The DLDD is an example of a device with high symmetry and is therefore a suitable candidate for computer simulation. Henrik Bruus and Martin Heller at MIC DTU modelled the flow of particles around obstacles [13] using a method known as the level set

method. Heller also modelled the behaviour of particles in DLDDs in his masters thesis [14].

2.2 Inducing flow

In order for flow to occur there must be a force applied to the fluid that exceeds the forces tending to stop flow. There are a variety of means by which forces can be applied, as previously mentioned, and these methods lead to different flow-profiles. The flow profile is the distribution of velocities of fluid elements across a channel. We will here highlight the differences between pressure driven flow, electroosmotic flow and the electrophoretic transport of particles through a medium.

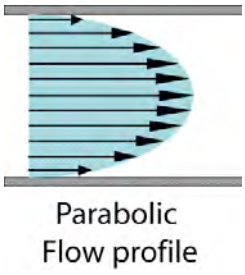

Figure 2.1. The arrows represent the velocities. The flow speed is zero at the walls and reaches its maximum in the centre of the channel.

2.2.1 Pressure driven flow

Pressure driven flow is created by a pressure difference ΔP between the inlet and outlet of a channel. There is a pressure difference between fluid-elements at different heights.

$$\Delta P_{gravity} = \rho \cdot g \cdot \Delta h$$

Where ρ is the fluid density, g is gravitational acceleration and Δh the height difference. We strive to keep channels horizontally oriented but for the sake of argument imagine tilting a channel so that one end is 5mm higher than the other. The pressure difference due to gravity will be:

$$\Delta P_{gravity} \approx 10^3 \left[kgm^{-3} \right] \cdot 10 \left[ms^{-2} \right] \cdot 0.05 \left[m \right] = 500 Pa$$

We will typically use $\Delta P_{pump} \approx 10^5 \, Pa >> \Delta P_{gravity}$ and therefore neglect gravitational-effects as previously mentioned. ΔP will be used to denote the pressure applied by a pump.

If we also neglect the inertial effects due to the acceleration of the fluid (this is possible because steady flow is achieved rapidly) then the flow rate will be determined by the relationship between the pressure drop and the resistance from the channel walls. Due to adhesion forces between the fluid and the channel walls, the flow velocity is zero at the boundary. Shear forces between layers of fluid slow the flow resulting in a parabolic distribution of velocities.

The flow rate Q [m^3s^{-1}] in a micro-channel is given by the formula

$$Q = \frac{\Delta P}{R}$$

Where R is the fluid resistance.

Fluid resistance is dependent on channel geometry. Two common cross sectional geometries are circular and rectangular and the resistances of these geometries are according to ref [15] given by,

If η is the viscosity, L is the length of the channel and r the radius of the tube then:

$$R = \frac{8\eta L}{\pi \cdot r^4}$$ For a tube of circular cross section

$$R = \frac{12\mu L}{wh^3}\left[1 - \frac{h}{w}\left(\frac{192}{\pi^5}\sum_{n=1,3,5}^{\infty}\frac{1}{n^5}\tanh\left(\frac{n\pi w}{2h}\right)\right)\right]^{-1}$$ For a rectangular channel with an aspect ratio approaching unity.

$$R = \frac{12\eta L}{w \cdot h^3}$$ For rectangular channels with high aspect ratio

The resistances of other geometries have been calculated in ref [16].

Although pressure is easily applied to channels via vacuum pumps, syringe pumps or even peristaltic pumps either external to or integrated within microfuidics devices [17] the limitations of pressure driven flow are immediately apparent from the equations above. Due to the dependence, $R \sim \frac{1}{r^4}$ or $R \sim \frac{1}{wh^3}$, it becomes increasingly difficult to generate the pressure drops needed to overcome the large resistances involved as the dimensions of channels decrease and enter the submicron realm. Even when these pressures can be generated they must be contained within the device.

Irreversible PDMS-PDMS or PDMS-glass bonds can withstand maximum pressures of between 2 and 3.5 bar [18]. The pump we use can generate 2.5 bar but syringe pumps can generate considerably higher pressures. The syringe pumps we have from World Precision Instruments can push with a force of 35lb, which with a syringe of 0.1 $inch^2$ means 350lb $inch^{-2}$ or 25 bar. In order to avoid mechanical failure we should remain below 2 bar.

One can of course imagine fabricating DLDDs in other materials, utilizing alternative bonding methods, which would result in more robust structures. The weak link when using PDMS is the strength of the bond between layers, a link that can be removed by using monolithic structures (see chapter 5). Brian Bilenberg of MIC DTU has fabricated DLDDs in Topaz [19] which can withstand higher pressures than PDMS. These structures cannot, on the other hand, be deformed and therefore tuning of the critical size could only be obtained through control of the direction of fluid flow.

A second alternative would be the encasing of PDMS devices in a supportive structure. In order to retain the ability to study the system optically, the support would need to be both

transparent and thinner than the working distances of the lenses used. Glass or PMMA would be the prime candidates.

In possible future applications of the DLDD, optical compatibility may not be necessary and the use of high pressures in devices fabricated in, for example steel, could give separations with extremely high throughput.

2.2.2 Electrophoresis

Charged particles experience forces when subjected to an electric field. These forces cause the particles to move at a velocity dependant partly on the size and sign of their charge but also on the frictional drag that varies due to the size and shape of the particles.

Figure 2.2. The forces acting on a particle suspended in a liquid and subjected to an electric field.

With the viscous drag force $F_{viscous} = fv$ and the electrostatic force $F_{electr} = q_{eff}E$ balanced, the velocity of the particle is constant,

$$v = \mu_{el} E$$

where μ_{el} is the electrophoretic mobility. Typical values for the electrophoretic mobility are for example:

DNA ~1μm/s per V/cm
Polystyrene beads ~2μm/s per V/cm

2.2.3 Electroosmosis

Nearly all surfaces are charged. This applies also to the surfaces of microfluidic channels that are in contact with the fluid. The surface charge attracts oppositely charged ions in the liquid causing them to congregate at the surface. Nearest to the surface, a layer of ions is formed that, due to the attraction to the charged wall is immobilized. This is known as the Stern layer. Beyond the stern layer, a mobile layer with an excess of charged ions with the same sign as the Stern layer forms. An electric field component parallel with the channel wall will pull the ions together with the liquid, via viscous interactions, through the channel. The velocity is given by the following equation:

$$V = \frac{\zeta \varepsilon_r}{4\pi\eta} \cdot E \qquad (2.1)$$

Where ζ is the zeta potential, ε_r the relative permittivity, E the electric field and η as always the viscosity.

There are two main benefits of using electroosmosis. The resultant velocity profiles are, with the exception of a small deviation at the channel wall needed to satisfy the non-slip boundary conditions, linear as opposed to the parabolic profiles generated by pressure driven flow. The flow rate is, as equation 2.1 shows, independent of channel size. This independence of the velocity on channel size means that electroosmosis is often used when the dimensions become too small for pressure driven flow to be implemented.

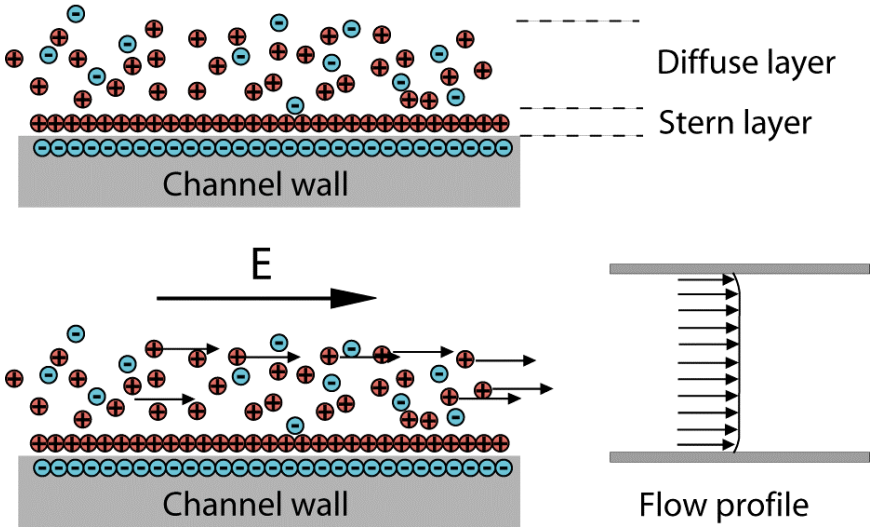

Figure 2.3. The charged surface of the channel walls attracts ions in the fluid creating the immobile `Stern´ layer and the mobile `Diffuse´ layer (above). The excess of charges in the diffuse layer moves in the presence of an electric field dragging along the bulk of the fluid via viscous interactions (below left). The distribution of flow speeds across the channel is more or less constant. There is a slight bending of the profile very near to the wall due to the no slip conditions causing zero flow speed.

Another limitation of electroosmosis is the fact that the velocity is dependant on wall zeta potential which due to contamination, adsorption of analytes and other surface inhomogeneities is often not constant throughout a device.

As we shall later see, PDMS can be treated with oxygen plasma in order to irreversibly bond together component layers or to seal channels with glass covers. The process also leaves the surface covered with a layer of silanol (SiOH) groups which become charged (SiO^-) in contact with neutral or basic solutions. This means that oxidized PDMS surfaces support EOF towards the cathode [20].

Electrophoretic and electroosmotic transport are always present to some degree when electric fields are used. It is often necessary to suppress one of the effects in order to use the other. If for example the EOF velocity, toward the cathode in a PDMS channel, is comparable with the velocity of negative particles toward the anode due to electrophoresis, then the particles could move in either direction. The electroosmotic flow can be suppressed by using methyl cellulose which forms brush-like structures on the channel walls inhibiting the movement of the diffuse layer and suppressing the zeta potential [21].

2.3 Laminar and turbulent flow

Under certain conditions, microscopic fluid elements follow well-defined paths known as *streamlines*. Any fluid elements entering a system at the same point will follow the same streamline through the entire system. This mode of flow, integral to the working of the DLDD array, is known as *Laminar flow*. At higher flow rates the streamlines begin to fluctuate and fluid elements no longer follow well-defined paths. This is the transition between laminar flow and *Turbulent flow*. Turbulent flow occurs when inertial forces dominate over viscous forces. The ratio between inertial and viscous forces, the *Reynolds number*, can be used to determine which mode of flow will dominate in a micro-fluidics system.

$$\mathrm{Re} = \frac{\text{Inertial effects}}{\text{Viscous effects}} = \frac{D_H \rho \langle v \rangle}{\eta}$$

Re = Reynolds number
D_H = Hydraulic diameter of the channel
ρ = Fluid density
$\langle v \rangle$ = Flow velocity
η = Viscosity

The hydraulic diameter of the channel is related to the ratio of the surface area to the volume and the geometry of the channel. It is calculated as "four times the cross-sectional area divided by the wetted perimeter" [22].

$$D_H = \begin{cases} d & \text{tube diameter in capillary tubes} \\ 2h & \text{slot height} \\ \dfrac{2}{\dfrac{1}{h} + \dfrac{1}{w}} & \text{for square channels with height } h \text{ and width } w \end{cases}$$

If the Reynolds number exceeds 2000 then the flow will be turbulent. A Reynolds number less than 30 guaranties laminar flow, and in the range 30 to 2000, the fluid can flow in either mode depending on the geometry of the system.

Channel widths in the case of the DLDD array can be taken as the gap between the obstacles (see chapter 4), which provided we have not deformed the device, are rectangular in form. Typical distances between posts are on the order of 20μm and as channel depth is also on this same scale the hydraulic diameter of our devices is more or less 20μm. In order to ensure laminar flow in our devices we should use flow speeds that ensure a Reynolds number less than 30:

With: Re=30
η=10^{-3}kgm^{-1}s^{-1}
d=20μm
ρ=10^{3}kgm^{-3}

the velocity is:

$$\langle v \rangle = \frac{\mathrm{Re}\,\eta}{d\rho} = \frac{1 \cdot 10^{-3}}{10^{3} \cdot 20 \cdot 10^{-6}} = 1.5 ms^{-1}$$

In order to reach the turbulent flow regime the velocity would need to be 70 times this (105ms^{-1})!

We can approximate the maximum velocity that is obtainable with the pumps we have at our disposal using the flow in a circular channel with cross sectional area A:

$$v = \frac{\phi}{A} = \frac{\Delta P d^2}{8\eta L}$$

Using the pump to suck fluid through the channel limits the maximum pressure to 1 atmosphere. The maximum velocity of water in a channel 10μm in diameter and 2cm long is 0.06ms^{-1}. Using the pump to push the fluid through the channel, we can achieve 2.5 times the pressure and therefore 0.15ms^{-1}. The latter value corresponds to Re=1.44 and we therefore assume that all flow in the DLDD´s will be laminar.

2.4 Diffusion

One of the consequences of laminar flow is that there will not be any mixing between streams flowing in contact with one another except by diffusion. Molecules vibrate due to their thermal energy and collide with each other in a random manner. The molecules collide also with larger particles in solution exerting randomly distributed forces upon them. Due to the random nature of these forces, the particles travel varying distances in different directions, the phenomena known as Brownian motion. Diffusion is the process in which Brownian motion drives concentrations toward equilibrium. The root mean square of the distance a particle can travel in one dimension in time t is dependent on the diffusion coefficient in the following way:

$$d^2 = 2Dt$$

The diffusion coefficient is given by the Stokes-Einstein equation [9].

$$D = \frac{k_B T}{6\pi\eta R_H}$$

Here k_B is Boltzmann´s konstant, T is the temperature, η the viscosity and R_H the hydrodynamic radius of the particle. Because of the quadratic dependence of the distance d, diffusion becomes highly relevant in micro-fluidics devices. An example of this is haemoglobin in water for which the diffusion coefficient D=7*10^{-7}cm^{2}s^{-1} [15]. A molecule of haemoglobin can diffuse a distance of 10μm in only 1 second but it would take about 3 months for the same molecule to diffuse a distance of 1cm. As a rule of thumb, the upper

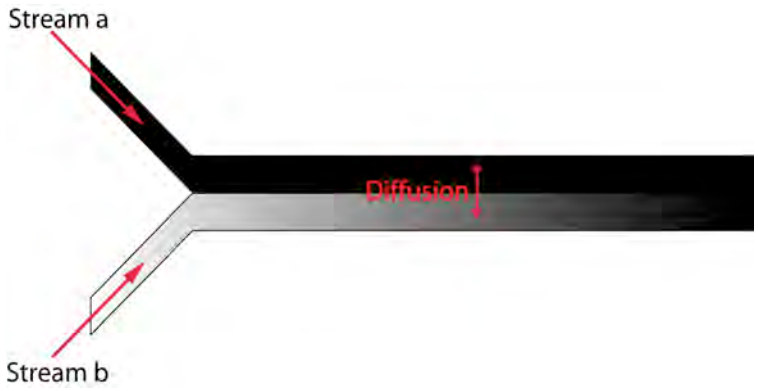

Figure 2.4. Mixing does not occur between two laminar flow streams except by diffusion. Given enough time the contents of the streams will mix completely. High Peclet numbers assure that this does not happen.

limit for diffusion coefficients is given by that for water molecules, which is approximately $10^{-5}cm^2s^{-1}$.

Because flow is nearly always laminar on the micro-scale there is no convective mixing due to turbulent flow and diffusion is the only mechanism by which mixing can occur. In some cases, mixing is desired and can be increased using channel geometries that maximize the surface area between streams [23-25]. In the context of separation, diffusion although used in methods such as exclusion chromatography, acts to limit resolution and should therefore be minimized. As will be discussed in the chapter covering the theory of separation, band broadening due to diffusion can be minimized by utilizing flows, although still in the laminar regime, sufficiently fast that the time taken for the particles to move through the separation device and therefore the time available for broadening is minimal. The Péclet number, defined as;

$$Pe = \frac{vd}{D} = \frac{\frac{v}{d}}{\frac{D}{d^2}} = \frac{\text{convective rate}}{\text{diffusive rate}},$$

where v is the flow speed, d the characteristic dimension of the array and D the diffusion coefficient of the particle being separated should be as high as possible to minimize the detrimental effects of diffusion in the DLDD.

2.5 The Radius of a Particle

How does one define the radius of a non-spherical particle, a protein for example? Some of the definitions of radii are as follows:

Radius of Rotation (R_R)*:* The radius of a sphere defined by rotating the protein about the centre of mass.

Mass Radius (R_M)*:* The radius of a hard sphere of the same mass and density as the protein.

Radius of Gyration (R_g)*:* The mass weighted average distance from the centre of mass to every atom in the protein.

Hydrodynamic Radius (R_H): The radius of a hard sphere that diffuses at the same rate as the protein.

The hydrodynamic radius takes into account the shape of the particle and the effects of hydration. R_H is given by the Stokes-Einstein equation as:

$$R_H = \frac{k_B T}{6\pi\eta D}$$

Experimentally measuring the diffusion coefficient allows the calculation of the hydrodynamic radius. Examples of the different radii for Lysozyme are shown in figure 2.5:

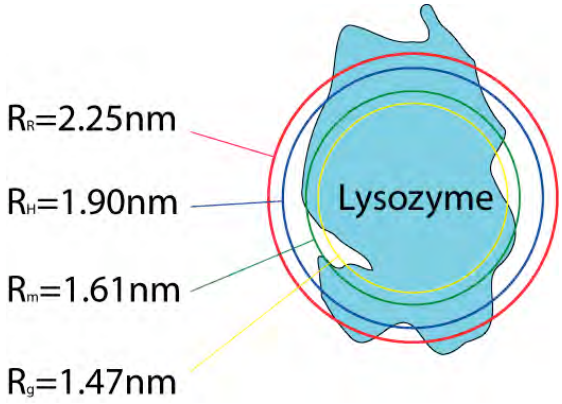

Figure 2.5. The image gives an idea of the different radii of the protein Lysozyme.

Depending on the structure of the particles, the centres of the spheres defined by these radii do not necessarily coincide. Which of these radii and centres of mass are important when considering the DLDD? The hydrodynamic radius is important as it determines the diffusion rate. It is also believed that the position of the hydrodynamic centre of mass determines which streamline the particles follow. On the other hand it is the physical extension of the particles that decides how far they are pushed to the side upon interaction with the posts and this extension may not be spherically symmetrical. The situation is further complicated by the fact that due to forces from the obstacles and shear forces from the carrier fluid the radii of non-rigid particles could vary as they move through the DLDD.

In the case of SAT it will be necessary to study the effects of protein adsorption on the different radii, R_x, of the beads used in the suspension arrays. Will R_x depend on the type of interaction used? Will they depend on the surface coverage of protein on the beads and if so will the effect be quantifiable and controllable? And will there be a difference if the proteins denature on the surface or if they retain their structure? Both experimentalists and theorists, in order for the DLDD to reach its full potential, must address these and other questions.

Chapter 3

Separation Science

In this chapter we will look at the ways in which separation techniques can be evaluated and compared with one another. We define both the *plate height* as a measure of the separative power of a device and the *resolution* and look at the relationship between these two numbers. In order to be able to compare the DLDD to other methods we will look at a few examples of commonly used separation techniques. Where not otherwise stated, the material is adapted from J Calvin Giddings book "Unified Separation Science" [9]

3.1 Number of Theoretical Plates.

One index commonly used to denote separation power is *number of theoretical plates N*. The number of theoretical plates is the number of discrete distillations that would have to be performed to obtain an equivalent separation. This number is commonly used as a measure of separation efficiency and is a useful number to use when comparing the performance of various chromatographic columns. Gas chromatography columns normally have 1,000 to 1,000,000 theoretical plates.

The variance of the Gaussian distributions of zones of particles being separated increases in time due to diffusion in the same manner as the root mean square of the individual particle migration distances:

$$\sigma^2 = 2D_T t \tag{3.1}$$

where D_T is the effective diffusion coefficient.

A zone will, if moving with constant velocity *v*, travel a distance *d* in time *t*.

$$d = vt \tag{3.2}$$

Substitution of (3.2) into (3.1) gives ,

$$\sigma^2 = 2D_T \cdot \frac{d}{v} = Hd$$

H, called for historical reasons *plate height,* expresses the rate of growth of σ^2 along the separation path. Evaluation of the plate height allows comparison of diverse zonal separation techniques.

The number of theoretical plates *N*, can then be defined in the following way:

$$N = \frac{d}{H} = \frac{d^2}{\sigma^2} = \frac{vd}{2D_T}$$

N shows how the efficiency of a zonal separation technique can predicted by looking at the speed at which the separation is run, the distance over which the separation takes place and the effective diffusion coefficient of the particles being separated.

According to our previous definition of the Péclet number:

$$N = \frac{Péclet\ number}{2}$$

3.2 Resolution

The term "resolution" can have a variety of meanings depending on the context in which it is used.

In optical microscopy the resolution is the smallest size difference that can be distinguished. When using an optical microscope to observe separations in the DLDD it is necessary to be able to resolve the separated zones.

The maximum resolution of a microscope is given by the diffraction limit in which the maximum in intensity of the light from one point coincides with the first minimum of the second.

$$d_{\min} = 0.61\frac{\lambda}{n \cdot \sin\theta}$$

d_{min} is the minimum distance between two points that can be resolved using light with a wavelength λ and a lens with a numerical aperture (NA) $n \cdot \sin\theta$

magnification	NA	d_{min} /μm
0.5	0.025	13.4
1	0.04	8.39
2	0.06	5.59
4	0.13	2.58
10	0.30	1.12
20	0.45	0.75
40	0.55	0.61
60 (water immersion)	1.00	0.34
60 (oil immersion)	1.40	0.24

Table 1. Resolution of the lenses at our disposal as a function of the numerical aperture (NA).

Table 1 shows a list of the lenses we have and the resolutions that can be obtained with them assuming that the average wavelength of light that we use to be 550nm. The working distance of the oil immersion lens is, at 0.21mm, less than the thickness of the PDMS and therefore too small for it to be compatible with our devices. Although resolution is almost always lower than the theoretical limit due to aberrations caused by non-ideal optical components, with the 60x water immersion lens we can theoretically resolve a difference in position of two particles of 240nm.

In the context of separation, resolution is used to denote the smallest difference in particle size that can be determined. The distribution in particles sizes is often Gaussian in form, the same as the distribution in the intensity of light and the resolution R_s, categorizes the overlap of two specified zones. If the centres of gravity of the two zones are found at X_1 and X_2 respectively then the resolution is defined as,

$$R_s = \frac{X_1 - X_2}{2(\sigma_1 + \sigma_2)},$$

where σ_1 and σ_2 are the standard deviations. Because the particles in the two zones do not differ greatly in size the standard deviations are assumed, to first approximation, to be equal giving:

$$R_s = \frac{\Delta X}{4\sigma},$$

with σ the average deviation. As the effective zone width $w = 4\sigma$ we can write,

$$R_s = \frac{\Delta X}{w}.$$

Fig 3.1 shows the appearance of two Gaussian distributions as ΔX increases, increasing the resolution.

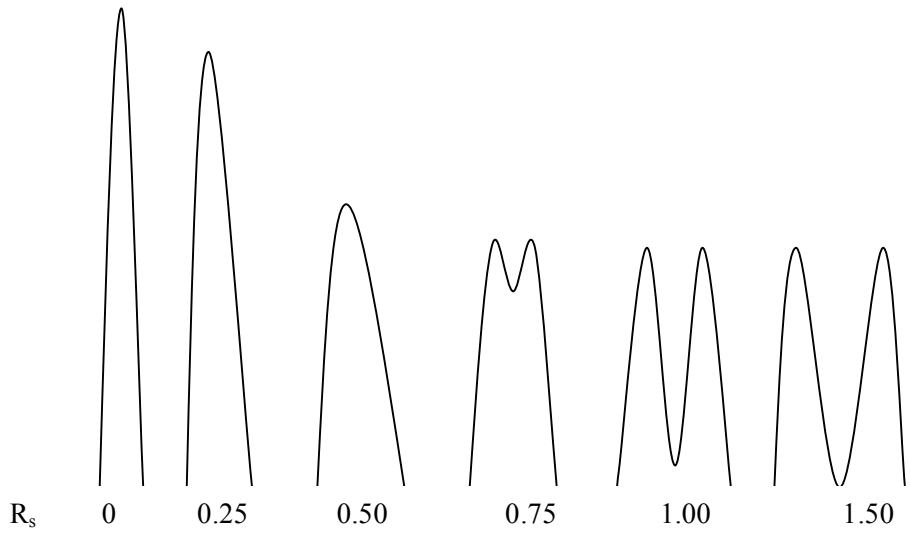

Figure 3.1. In order to clearly resolve two Gaussian distributions the resolution should be at least 1.

It is just possible to resolve two peaks when the resolution is 0.5 but a resolution of at least 1 is desirable.

3.3 Resolution and plate height

If we substitute $\sigma = (Hd)^{\frac{1}{2}}$ into equation *x* then we get,

$$R_s = \frac{\Delta X}{4(Hd)^{\frac{1}{2}}}$$

We see from this how the resolution increases with decreasing plate height.

3.4 Separation Techniques

Until recently, two-dimensional separation and analysis of proteins was most commonly achieved using two-dimensional gel electrophoresis (2-DE). In the first dimension proteins are separated according to their charge or isoelectric point, and in the second dimension by their molecular masses by sodium dodecylsulphate-polyacrylamide gel electrophoresis, (SDS-PAGE).

3.4.1 Electrophoresis

Electrophoresis utilizes the difference in the electrophoretic mobilities (see chapter 2) of ions (especially polyions) to cause separation. Electrophoresis is used widely in biochemistry for separation and analysis of such ions as e.g. amino acids, nucleotides, proteins, nucleic acids, proteoglycans etc. Electrophoresis is a versatile separation method because the electrical charge on the polyelectrolyte ions can be modified by change of pH

and even if the species being separated have the same electric charge, differences in molecular size and conformation affect the mobility because these factors determine f.

There have been many refinements in the field of electrophoresis leading to improved separation techniques such as capillary electrophoresis, 1 and 2D-gel electrophoresis, SDS-PAGE and isoelectric focusing to name a few.

3.4.2 Chromatography

Chromatography is, due to its outstanding separation power and versatility the most widely used of all separation techniques. The basic mechanism of chromatography is a differential retardation caused by unequal degrees of interaction between substances washed along in a stream of liquid and the stationary phase through which they flow. Figure 3.2 shows a schematic of a typical chromatography setup.

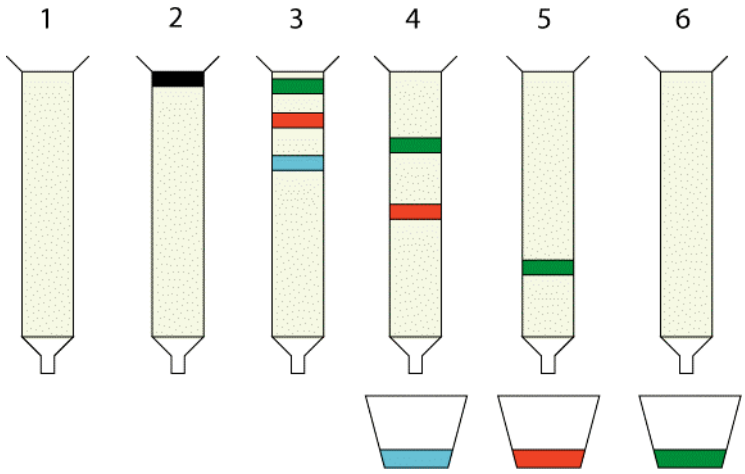

Figure 3.2 shows the basic principle behind chromatography. 1. Column with stationary phase. 2. The sample plug is introduced. 3. As the sample travels through the column zones are formed. 4,5 and 6. The separated particles can be collected.

The configurations used in chromatography, based on different combinations of moving and stationary phases and the interactions between them, now number in the hundreds. There follows here a brief description of a few of the most common of them.

Adsorption Chromatography – retardation is caused by adsorption on granular solids or other fixed surfaces.

Partition Chromatography – an absorbing liquid is held in place, within the pores of solid particles.

If a solid that retains some adsorptive qualities is used as a support for an absorbing liquid, a mixture of the above will be the result.

Ion-exchange Chromatography – beads have ionic groups that can change positions with ions in the mobile phase causing retardation.

Size Exclusion Chromatography - exclusion is induced by a porous support. The larger the molecules in the mobile phase, the less entropy they lose upon entering the pores of the beads in the stationary phase. The smaller molecules are free to diffuse around inside the beads, the result being, that they take a longer path through the column. See figure 3.3.

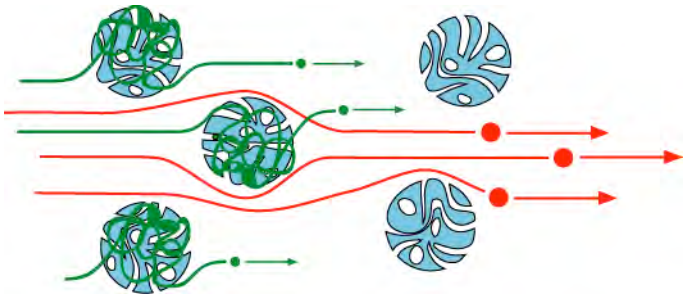

Figure 3.3. The smaller, green beads can diffuse into the pores of the packing effectively lengthening to migration path. The larger, red beads do not fit into the pores as well and therefore spend more time in the flow between the packing beads thus travelling a shorter distance. The result is separation between green and red particles (small and large) but also broadening of the bands as the routes taken vary even among particles of the same size.

Hydrodynamic Chromatography - the speed of flow, v, due to a pressure difference is given as a function of the distance from the channel wall, r, by:

$$v(r) = v_{\max}\left(1 - \frac{r^2}{a^2}\right)$$

where a is the channel radius.

Due to the parabolic profile, particles have different velocities depending on their position in the channel, and a plug of material travelling in the channel will spread out. This is detrimental to the resolution of a separation, but it can also be used to separate particles by size. It is the position of the hydrodynamic centre of mass that determines a particles velocity and since larger particles are excluded from the area near the wall, they spend more time in the faster central flow. *Hydrodynamic Chromatography* is the name given to separation by this method.

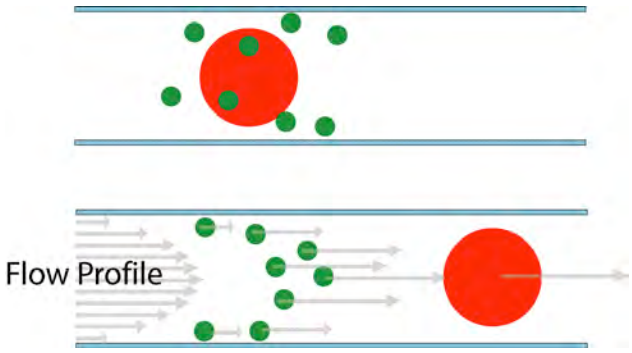

Figure 3.4. The large, red particle spends most of its time in the centre of the channel where the flow velocity is greatest. The smaller, green particles can diffuse laterally spending a higher fraction of their time in the slower moving liquid near the channel wall.

3.4.3 Field Flow Fractionation

Field flow fractionation (FFF) is a technique well suited to the separation of particles as diverse as cells, macromolecules, colloids and proteins. The basic mechanism is the application of a force, for example an electric field or gravity to drive particles towards a channel wall called the accumulation wall, (see figure 3.5). Depending on the force from the field and the effects of diffusion the particles reach steady state distributions close to the wall in a process called relaxation. The distributions are exponential in form and have a mean thickness given by,

$$l = \frac{D}{w}$$

Here *D* is the diffusion coefficient and w is the field-induced velocity. Because D and w are dependent on the characteristics of the individual particles the layers formed are of different thicknesses. Due to the parabolic flow profile, layers will have different mean velocities depending on there mean thicknesses and zones are formed along the channel.

Some of the driving forces used and the names given to the techniques are:

Electric field – ElFFF
Centripetal forces – sedimentation or SdFFF
Temperature gradient – Thermal or ThFFF
Cross flow – flow or FlFFF

For a more in-depth discussion of the field of FFF we refer the reader, again, to Giddings [9] or a more recent review article by Wolfgang Fraunhofer [26].

As we will see, deterministic lateral displacement can be considered a type of FFF.

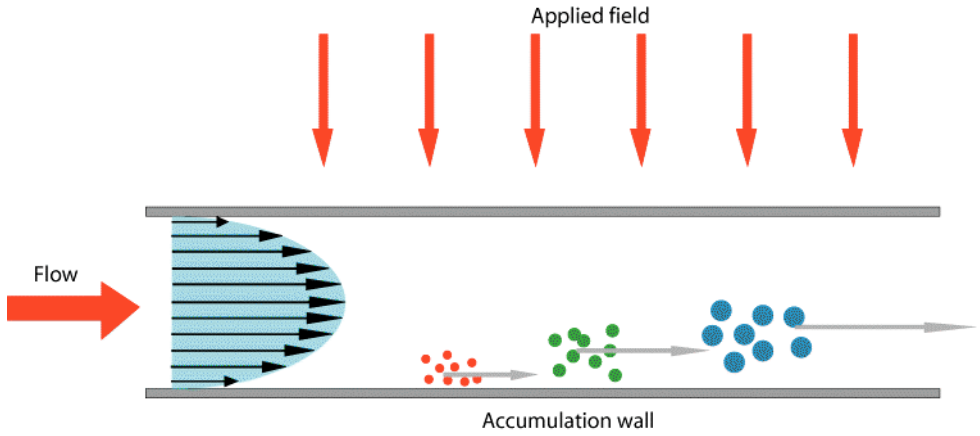

Figure 3.5. In the method known as Field Flow Fractionation the applied field drives the particles toward the accumulation wall. The particles relax into layers of different thicknesses and are subjected to different flow speeds due to the parabolic flow profile.

3.5 Conclusion

Common to all the methods of separation mentioned above is their reliance on diffusion. In many cases optimizing the performance of a separation method is a balancing act, in which enough diffusion to ensure separation is allowed while simultaneously minimizing zonal spreading, which is caused by excess diffusion. The time taken for particles to diffuse ultimately sets the limits on how fast these methods can be.

DLD differs from these methods in the sense that it is not dependent on diffusion. The limits as to how fast separations can take place are set instead by the condition that fluid transport should be in the laminar regime. Resolution actually increases with faster running speeds.

Chapter 4

Deterministic Lateral Separation

We will now show how obstacles in a microfluidics channel can be so placed as to divide a laminar flow into well-defined streamlines. These same obstacles apply a force, perpendicular to the direction of fluid flow, that selects which streamlines particles suspended in the fluid will follow. This pushing of particles into streamlines constitutes the driving force already mentioned in conjunction with FFF.

4.1 Geometry of the DLDD

The DLDD in the configurations that we have utilized, see fig 4.1, consists of a channel on the order of 2-3mm wide, 10-50μm deep and approximately 2cm long that defines the direction of flow ϕ, which is parallel with the channel walls. The channel is filled with an array of circular posts with centre-to-centre spacing, λ, tilted at an angle θ to the direction of flow. The angle θ is chosen such that each row is displaced perpendicularly to the direction of flow by $\Delta\lambda$. The relationship between λ, $\Delta\lambda$ and θ is,

$$\tan(\theta) = \frac{\Delta\lambda}{\lambda} = \frac{1}{N}$$

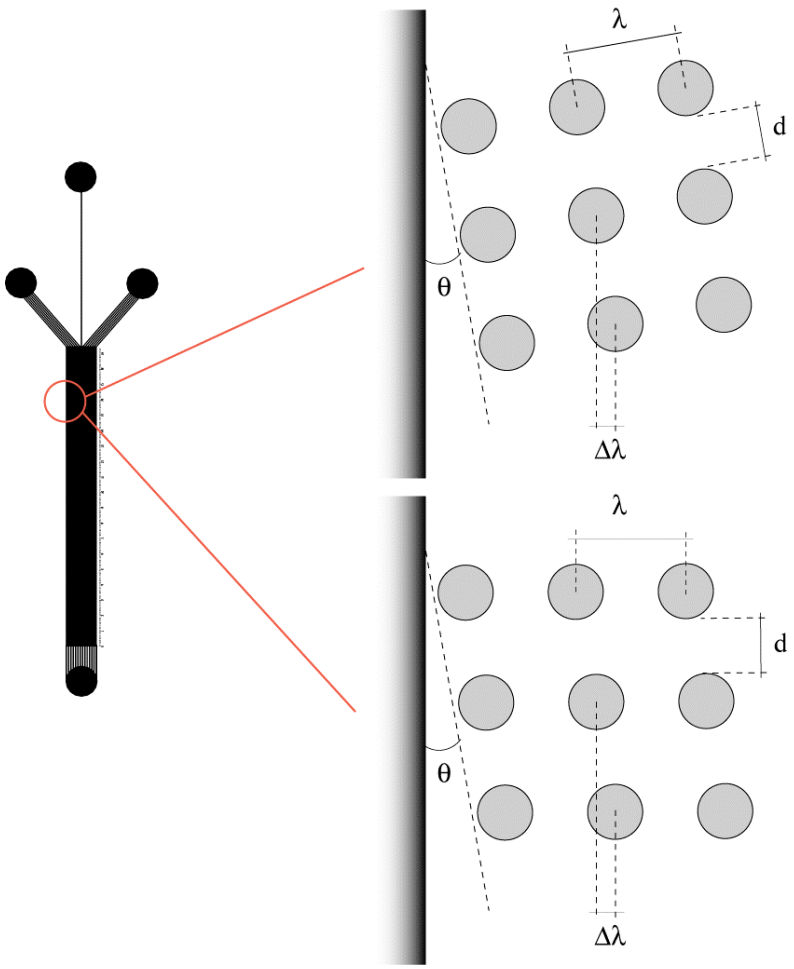

Figure 4.1. Two different geometries for the post arrays. The angle θ and the shift Δλ are the same in both designs but the distance between posts, as seen by the particles differs in the two cases.

Although there is no advantage, as we understand it, in using either one of the two geometries as opposed to the other, we have chosen to use the tilted quadratic array due to it being easier to produce with graphics software. We define therefore the period of the post array as

$$N = \frac{\lambda}{\Delta\lambda}.$$

If we define the coordinates y as the distance along the channel and x as the position perpendicular to the channel wall then we see that the x coordinate of posts is repeated cyclically with the period N.

4.2 Fluid Flow in the DLDD

As previously mentioned the flow in the DLDD is laminar and fluid elements follow therefore deterministic paths through the post array. We consider the fluid emerging from between two posts: On reaching the next row the fluid will divide and flow around the posts. In order for the average direction of flow to remain parallel with the channel walls

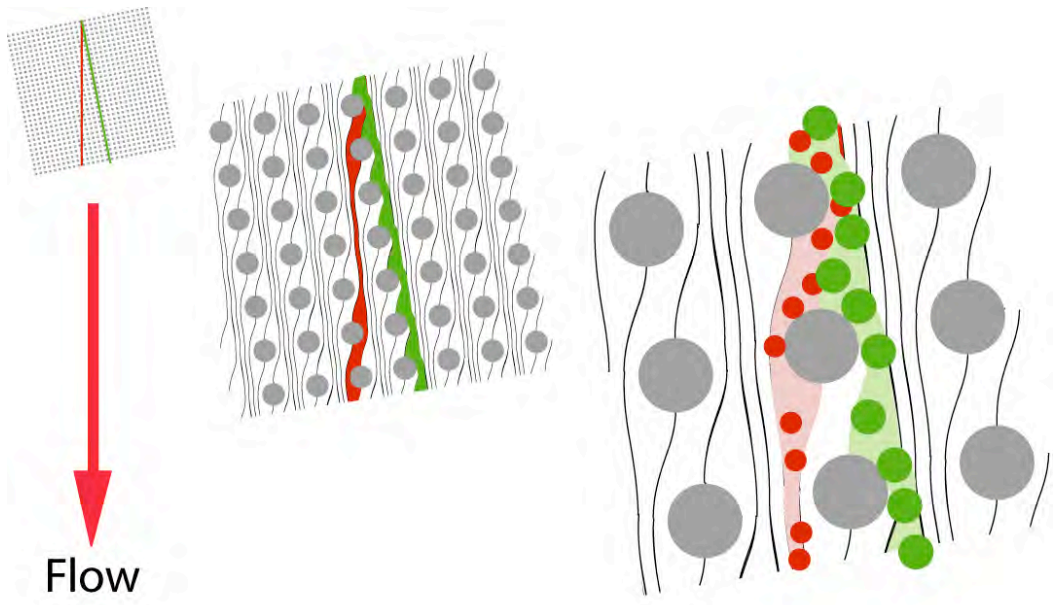

Figure 4.2. The red particles are smaller than the critical size and are able to follow the flow, zigzagging between posts, and move directly downwards in the image. The green particles are larger than the critical size and are therefore pushed across one stream to the right at each interaction with a post. The result is that the green particles move along the "corridor" created by two rows of posts.

the fluid must divide so that 1 part flows to one side of the obstacle and N-1 parts flow to the other. If we divide the space between two posts into N slots, numbered 1, 2, …, N-1, N, then we see that a streamline passing first through slot N will in the following row pass through N-1 and then through N-2 and so on until it arrives back at slot N. see fig 4.2.

4.3 Particle separation in the DLDD

Because the flow is laminar, inertial effects can be neglected and particles in suspension will follow streamlines. It is the position of the hydrodynamic center-of-mass of the particles that determines which streamline they will follow. Depending on the size of the particles, they will negotiate the post arrays in either of the following modes.

Particles with a hydrodynamic radius less than the slot width will remain in one streamline and describe the same path as fluid elements as they move through the channel.

If the hydrodynamic radius of the particle is larger than the width of the slots then it will not be able to remain in the same streamline. When the streamline passes through slot 1 the post will push the particle into the next streamline to the right. This streamline will pass through slot 1 at the next row whereby the particle will again be pushed one streamline to the right. This is repeated at every row. The net effect is that the particle will migrate at the same angle as the matrix rotation θ relative to the direction of flow.

We will adopt the terms "zigzag mode" and "displacement mode" respectively, used by L R Huang [1].

4.4 Calculating the critical radius

The critical radius R_c is determined by the slot width. For a blunt flow profile, in which the velocities are independent of *x*, the slots are all the same width and R_c is given by,

$$R_c = \frac{d}{N}$$

In reality, the flow profile between the posts is parabolic. The flux, ϕ, equal to the velocity times the cross section, is a conserved quantity which means that the cross sectional area of the streamlines increases as the velocity decreases. The width of the first slot will therefore increase. The parabolic flow profile is compensated for by the correction factor α and the critical radius becomes,

$$R_c = \alpha \frac{d}{N}$$

4.5 Calculation of the correction factor

We can calculate an approximate value for the correction factor in a 2D model. We approximate the posts with infinite plates at a distance d from one another, and define the coordinates *x* and *y* as before. See fig 4.1.

The parabolic velocity profile is given by:

$$v_y(x) = \frac{4v_{\max}}{d^2}\left(dx - x^2\right)$$

If we assume a device with depth $w >> d$, the partial flow ϕ between one plate and a plane a distance λ from that plane is:

$$\phi(\lambda) = w\int_0^{\lambda} \frac{4v_{\max}}{d^2}\left(dx - x^2\right)\partial x$$

The relative flow of the first stream is given by:

$$\phi_{rel}(\lambda) = \frac{\phi(\lambda)}{\phi_{total}} = \frac{w\int_0^{\lambda} \frac{4v_{\max}}{d^2}\left(dx - x^2\right)\partial x}{w\int_0^{d} \frac{4v_{\max}}{d^2}\left(dx - x^2\right)\partial x} = 3\left(\frac{\lambda}{d}\right)^2 - 2\left(\frac{\lambda}{d}\right)^3$$

If we now take $\phi_{rel}(\lambda) = \frac{1}{N}$ and $\lambda = R_c$ we see that,

$$\frac{1}{N} = 3\left(\frac{R_c}{d}\right)^2 - 2\left(\frac{R_c}{d}\right)^3 = \frac{R_c^2}{d^2}\left(3 - 2\frac{R_c}{d}\right) \approx \frac{R_c^2}{d^2}\left(3 - 2\frac{\alpha}{N}\right) \Rightarrow$$

$$\text{(for large N)} \Rightarrow \frac{1}{N} \approx 3\left(\frac{R_c}{d}\right)^2 \Leftrightarrow R_c^2 \approx \frac{d^2}{3N} \Leftrightarrow R_c \approx \frac{d}{N} \cdot \sqrt{\frac{N}{3}} \approx \frac{d}{N} \cdot \alpha$$

So the correction term is approximately:

$$\alpha \approx \sqrt{\frac{N}{3}}$$

Which gives α=1.8 for a period of 10.

In our devices we do not actually have *w>>d* and so the correction factor should be somewhat larger.

In 3D the correction factor will depend on the particles height in the flow. Martin Heller at DTU has calculated, numerically, α as a function of position in the array *see reference [14]*. Table 2 shows Hellers results.

2z/h	0.0	0.1	0.2	0.3	0.4	0.5	0.6	0.7	0.8	0.9
α (N=10)	1.431	1.442	1.448	1.460	1.485	1.512	1.561	1.626	1.719	1.838

Table 2 Correction factors at different positions in the DLDD. The relative position 2*z/h* is given with respect to the centre of the channel. *With kind permission of Martin Heller [14].*

We have measured α experimentally for devices in which $w \approx d$ and find it to be about 2.5. In the theoretical calculations it is assumed that the critical radius is the same as the width of the first stream. The disagreement between the experimental and theoretical results could have its origins in the fact that this is not actually the case. This could be because the hydrodynamic radius of particles is not a very well defined property.

4.6 Scaling

The DLDD is still in its infancy. Although most work has been done on plastic beads, DLDD´s have also been used to separate white and red blood cells [21]. As far as we know only particles in the 0.1 to 1μm range have been separated but there are no fundamental reasons why the DLDD cannot be scaled down considerably, allowing the continuous and rapid separation of sub 100nm particles.

There are several issues to consider when contemplating the downscaling of the DLDD´s.

- Decreasing *d* allows for the separation of smaller particles but also increases the fluid resistance decreasing the flow rate for a given pressure. Eventually pressure driven flow will not be practical.
- Lower flow rates mean the particles have more time to diffuse leading to greater tonal broadening and lower resolution.
- Increasing *N* gives smaller R_c but at the cost off a smaller ΔX meaning also lower resolution *see figure 4.3*.

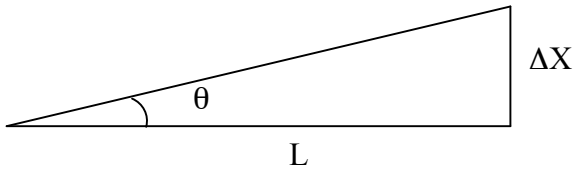

Figure 4.3 Particles moving at an angle θ through a DLDD of length *L* are separated by *ΔX*.

The maximum period *N* that can be used is limited by the resolution of the microscope (if one wants to observe separation).

$$N_{\max} = \frac{L}{\Delta X_{\min}} = \frac{20 \cdot 10^{-3} m}{340 \cdot 10^{-9} m} \approx 60000$$

This would mean that one could separate extremely small particles with large devices.

$$R_{c\min} = \alpha \frac{d}{N_{\max}} = \alpha \frac{d \cdot \Delta X_{\min}}{L}$$

Unfortunately as the angle $\tan\theta = \frac{1}{N}$ approaches 0 the device would become extremely sensitive to any small fluctuations in the direction of laminar flow and the zone broadening would make the device useless.

We have calculated the approximate dependence of the resolution on *d* and *N* [Appendix A] and find it to be:

$$R_s = C \cdot d^{\frac{3}{2}} \cdot N^{\frac{-5}{4}}$$

where $C = \sqrt{\frac{6\pi\Delta P}{32\sqrt{3}K_B T}} \approx 9.1 \cdot 10^9$

This calculation is done assuming a very narrow, delta function like, initial stream of particles. In reality the particles are injected in a stream of finite width so there is already broadening before the particles enter the separation area.

Further investigations into how scaling effects DLDD´s, primarily into how small *d* can be made and how large *N* can be, are necessary in order to determine how small the cutoff, R_c, can realistically be.

Chapter 5

Design Considerations

Apart from designing the geometry of the post arrays to separate specific sizes there are various other considerations. The primary concerns are the creation of laminar flow, injection of the samples in as narrow a stream as possible to increase the resolution (see chapter 3) and ensuring the migration of particles through the devices without clogging.

5.1 Laminar flow and focusing

As mentioned in the previous chapter, the width of the initial stream of particles entering the separation device adds to the total broadening thus reducing resolution. It is therefore important to inject particles in as narrow a stream as possible. Sample streams can be made narrow using hydrodynamic focusing [43,44]. The focusing of samples into streams as narrow as 50nm have been reported by R H Austin *et al* [43]. Figure 5.1 shows how control of the flow rates in the buffer (side) channels allows contol of the width of the sample stream. The additional channel walls have the added benefit that they give mechanical support to the channel roof preventing possible collapse.

The focusing occurs because the velocity across the wide area where the channels meet must be constant and the width of streams changes in order for this criterion to be met. However, the velocity of the central stream cannot change instantaneously and there is therefore a bloomimg or bulging of the stream upon entering the wider area. Although the stream later becomes narrow zone broadening would already have occurred at the entrance to the obstacle array area. In reference [44] Austin *et al* show how bulging in focused streams can be avoided by dividing the sheath flow into many narrow flow streams by dividing channels into narrow sub-channels *see figure 5.2*.

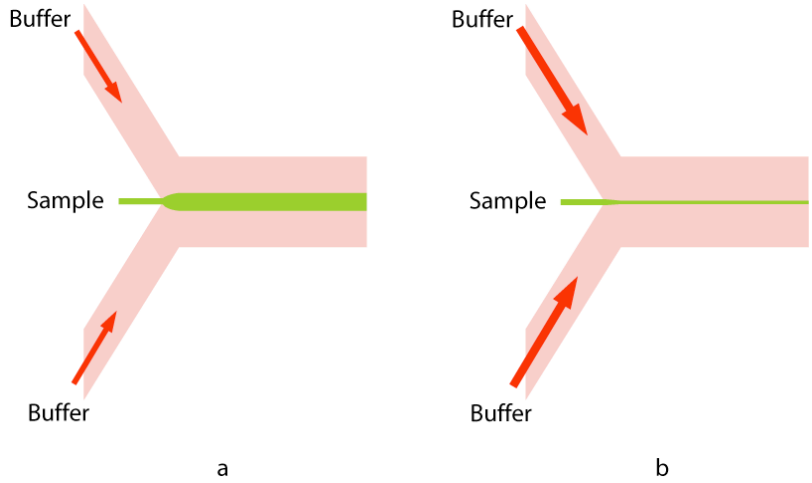

Figure 5.1 a) Higher pressure in the sample stream than in the sheath flow of buffer solution leads to a broadening of the stream which could mask small spatial separations in the DLDD. **b)** By utilizing higher pressure in the sheath flow the sample stream can be focused.

5.2 Clogging

One of the problems that need to be overcome is the blocking of the entrance and exit channels and of the post array itself in the DLDD. There are three main reasons for the blockages to occur.

- The particles, or agglomerates of particles, are too large to negotiate the post array, and become stuck between the posts. This occurs mainly at the entrance to the post array. This can be overcome by using both deep channels and large periods, the later of which allows the gaps between obstacles to be as large as possible for the desired cutoff size.
- Interactions between the particles and the surface of the DLDD can also lead to blockages. Passivation of the surface can be achieved by pre-treatment with a range of substances depending on the particles being separated. The adsorption of proteins can be blocked by first flowing a solution of bovine serum albumin, BSA,

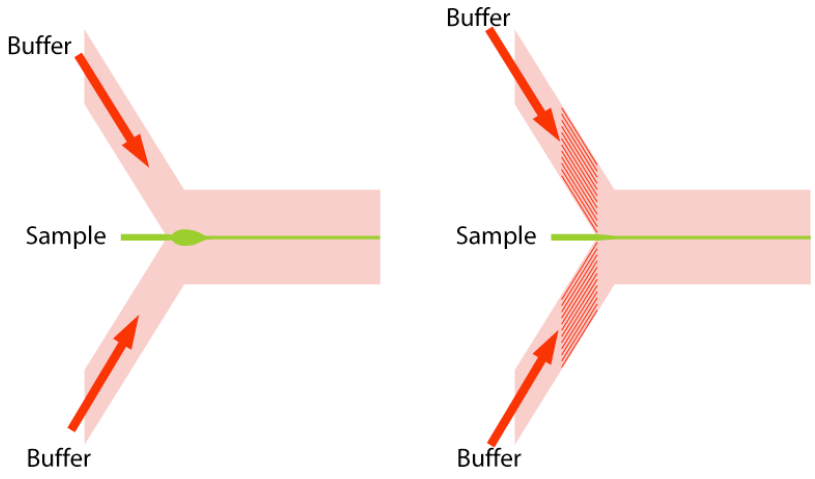

Figure 5.2 a) In a device three injection ports there is always a bulge in the central stream upon entrance to array area **b)** By dividing the wide channels into many narrower sub-channels the bulging of the central stream can be avoided. *See* ref [44] Mechanical support of the channel roof is also achieved.

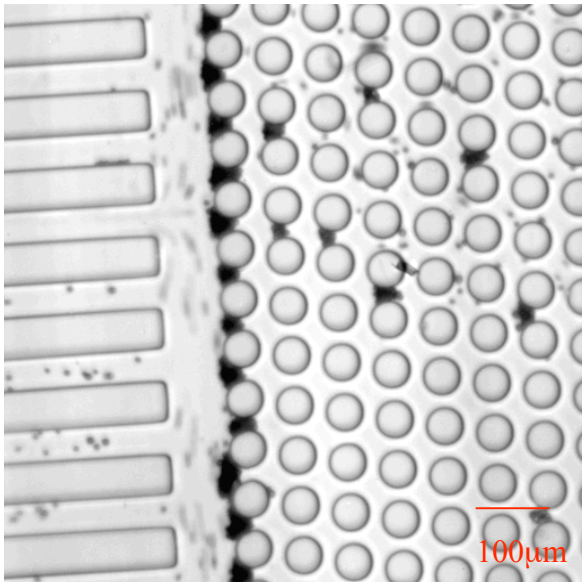

Figure 5.3 Agglomerations of beads have become trapped between the posts. This has occurred mainly it the entrance to the post array. The use of SDS in the buffer greatly improved the functioning of the devices by inhibiting the formation of groups of beads and by minimizing adhesion to the channel walls.

through the device. PLL-PEG has also been successfully used to passivate surfaces against protein binding [27]. Although it would not be compatible with biological samples, we found that the use of a 0.1% solution of a detergent, sodium dodecyl sulphate (SDS) in deionised water stopped both the agglomeration and the sticking of beads in the channels.

- In the DLDD there are areas where the flow speed is zero. Beads can enter these stagnant areas by diffusion and become trapped (see fig 5.4). This could be overcome by changing the shape of the posts to effectively fill the area of zero flow with post instead of fluid. Martin Heller at DTU is currently modelling the effects of post geometry on the areas of stagnation to see if they can be eliminated, or at least minimized, *see figures 5.5 and 5.6*.

These three mechanisms are of course closely connected to each other. In order for binding to occur, the particles need to be in contact with the channel walls for a length of time, depending on the kinetics of the interaction. Particles that enter an area of low flow speed spend more time near the surface and are more likely to bind. The shear force from the fluid is also less in areas of low flow speed and particles, once stuck, are less likely to be pulled free.

Once particles have begun to stick then constrictions form and more particles can be trapped either because they do not fit through the constricted gaps or due to the formation of new stagnant zones because flow is redirected.

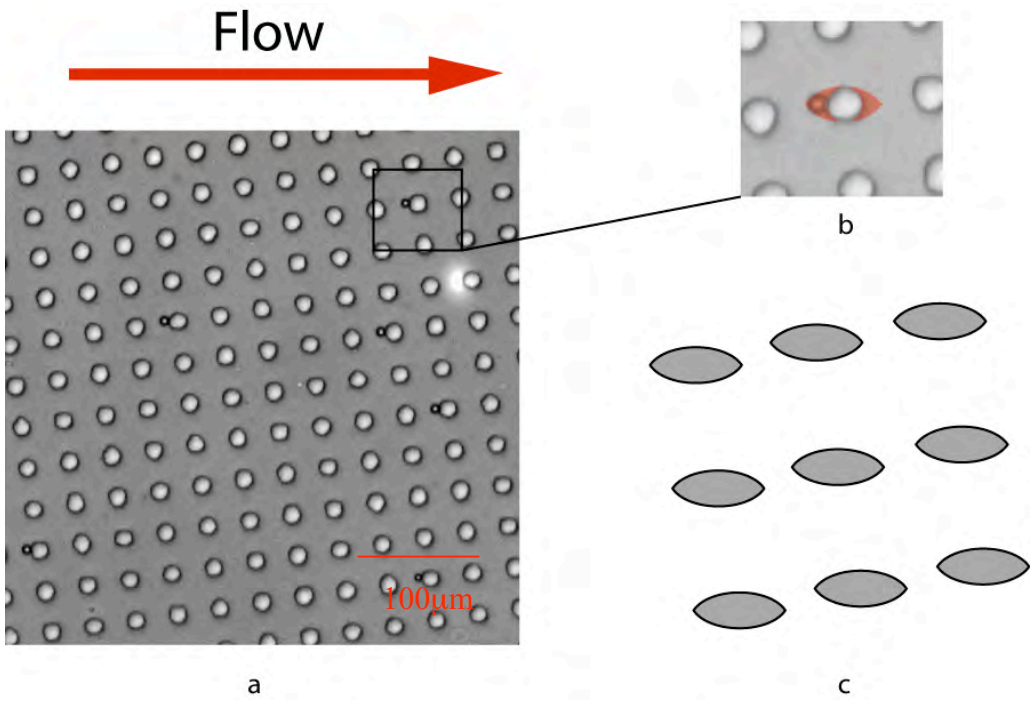

Figure 5.4 a) We found that beads tended to stick in the same positions relative to the posts. As far as we can tell, this is because the bifurcation of the flow around the posts leaves an area where the liquid is stationary, or stagnant. Beads seem to become trapped in these stagnant areas. **b)** The red highlight shows the suspected form of the stagnant area. **c)** Streamlining the shape of the posts could decrease the size of the stagnant areas sufficiently to prevent the trapping of particles.

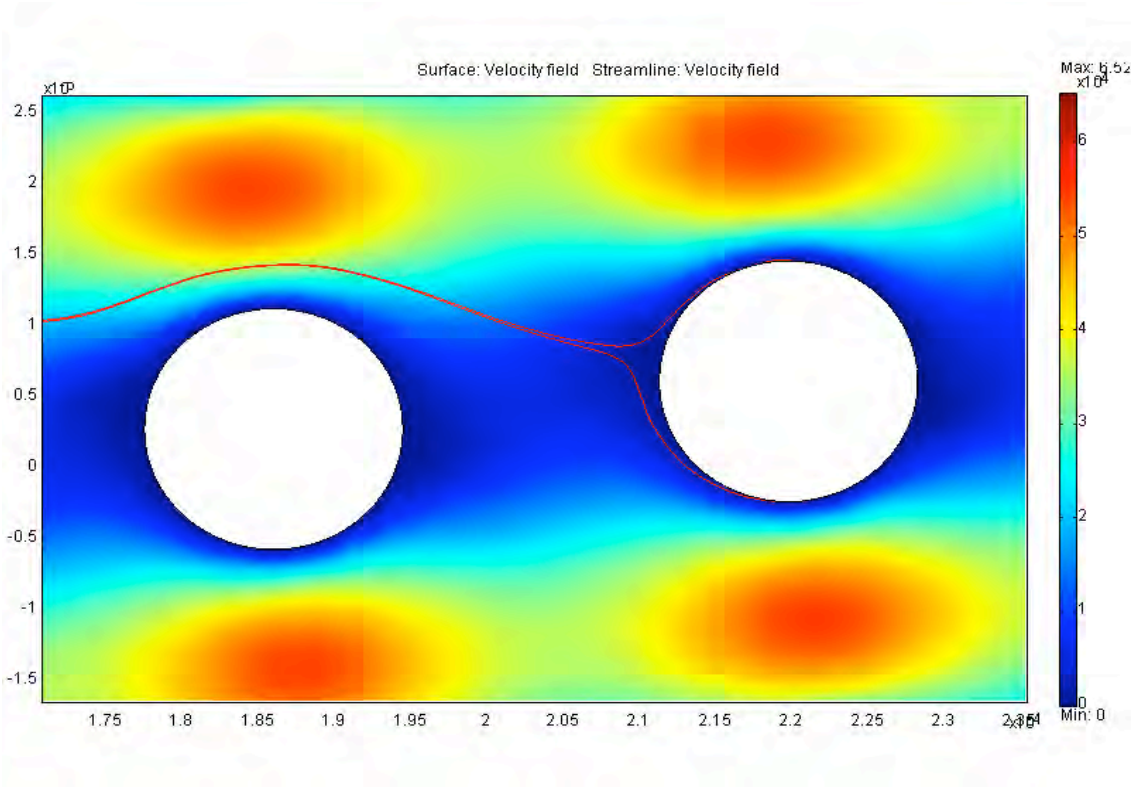

Figure 5.5 The stagnant zones are seen hear, in the close-up, in dark blue. The red lines are streamlines. *Image by kind permission of Martin Heller [14.]*

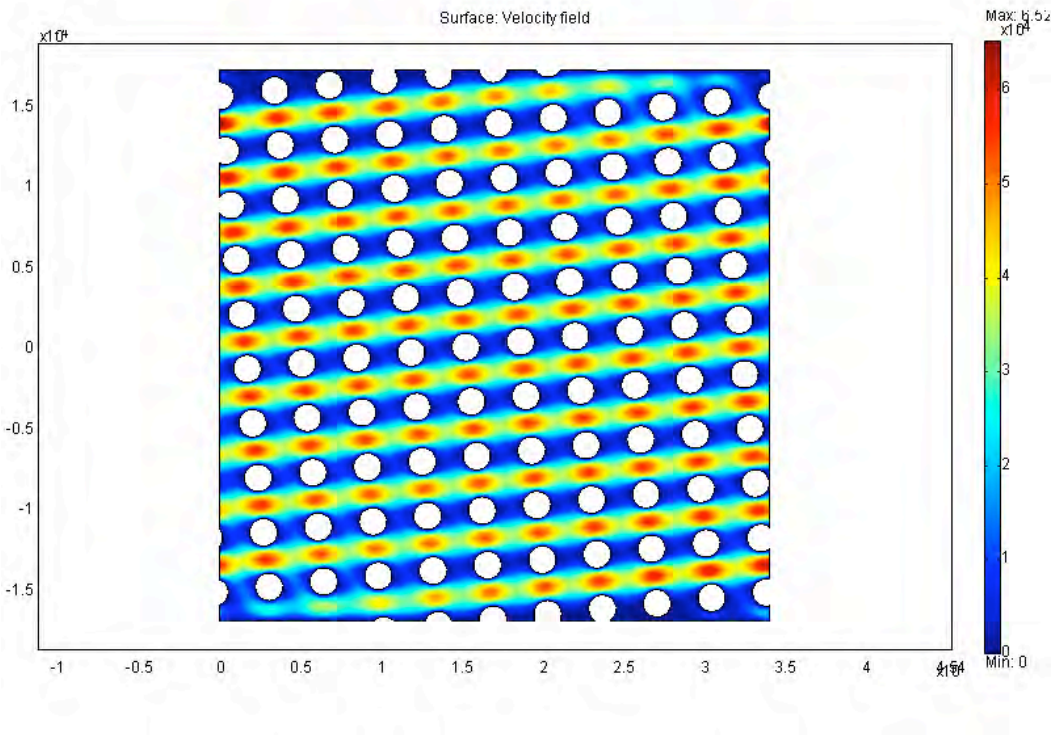

Figure 5.6 The image shows flow speeds calculated in a 2D Femlab simulation by Martin Heller. Red denotes areas where the flow is maximum and dark blue shows areas of low flow speed. *Image by kind permission of Martin Heller [14].*

Chapter 6

Fabrication

Poly (dimethylsiloxane) was chosen as the material from which to make the DLDD devices. Apart from the elastic properties that we intended to take advantage of in the stretcher experiments, PDMS is relatively cheap, compatible with many methods of optical detection due to its transparency between 230nm and 1100nm, biologically compatible, permeable to gases and impermeable to water.

Another of the advantages of PDMS is the speed at which designs can move from the drawing board to prototype, working devices using the technique known as replica moulding [18, 20, 28, 29]. UV lithography was used to make bas-relief masters in SU-8 spin coated onto silicon wafers [30]. After treating the masters with fluorinated silanes to prevent irreversible bonding [31], un-polymerized PDMS was poured on the master, cured and removed. The time taken to fabricate our devices was more often than not limited by queues to the equipment rather than pure fabrication time, and devices were at times realized in one working day.

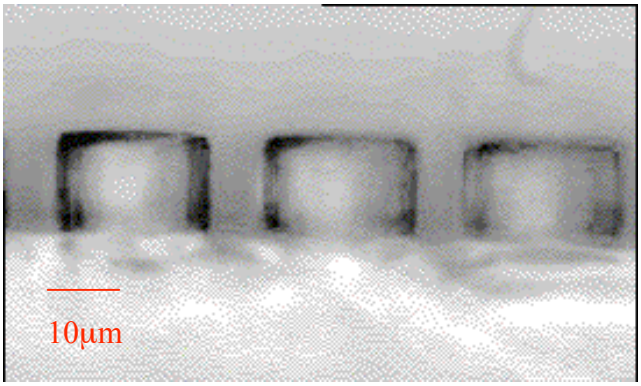

Figure 6.1 shows a cross sectional image of the posts in a DLDD. The PDMS was cut with a scalpel and the image taken in an optical microscope. The gap between the posts is actually the same as the post diameter (17µm) but appears to be less due to the angle at which the cross section was cut.

PDMS is hydrophobic. It can be very difficult to introduce aqueous solutions into hydrophobic channels without trapping air bubbles that disrupt flow, block channels and lead to devices that function poorly if at all. The surfaces of PDMS devices are easily made hydrophilic by treating them with oxygen plasma [32].

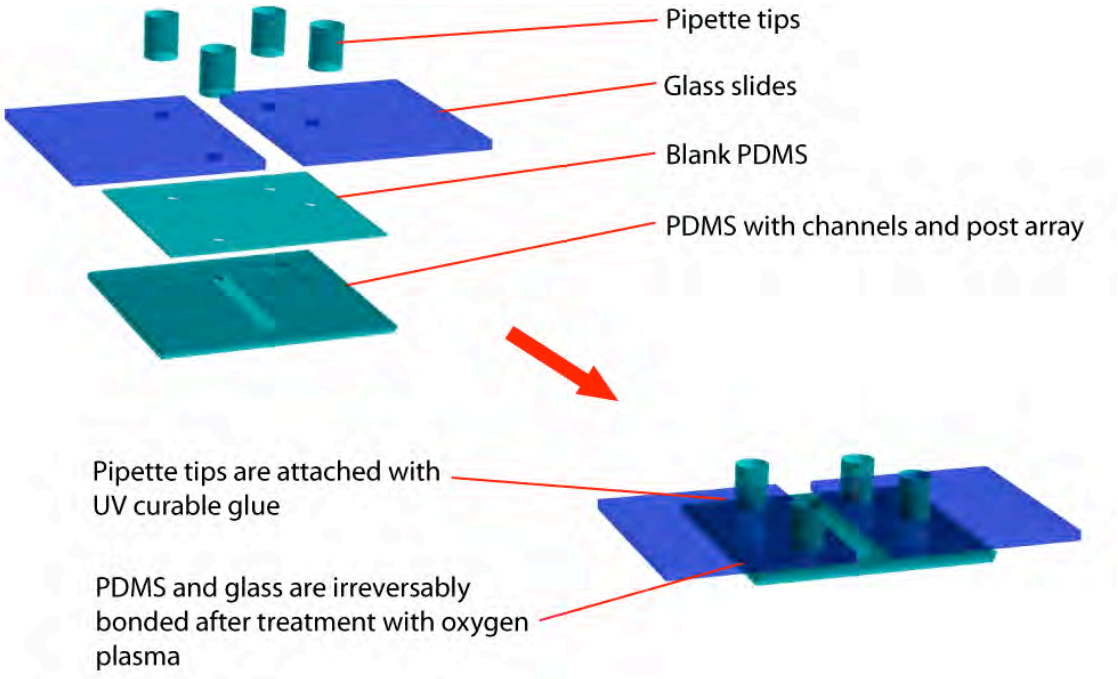

Figure 6.2 The post array and channels are defined in a slab of PDMS by replica moulding. A blank is cast and holes punched in it. Holes are etched in glass slides using a micro-sand blaster (Microetcher™, Denville Materials) and 50µm aluminium oxide. Cut-off pipette tips serve as reservoirs. The reservoirs are attached to the glass using UV curable glue (Norland Optical Adhesive from Norland Products, inc.) and the glass and PDMS components are assembled as shown in the figure after treatment with oxygen plasma.

Such oxygen plasma treatment also makes possible the bonding of PDMS to Si-based materials such as glass [20, 33, 34] or in the case of the stretcher to PDMS, via O-Si-O covalent bonds, in order to achieve closed channels. The bonding of devices using oxygen plasma requires some dexterity. The layers have to be removed from the plasma oven,

aligned and brought into contact correctly at the first attempt. This has to be done relatively quickly as the oxidized surface decays in between 15 minutes to one hour due to the diffusion of polymer molecules to the surface [32]. PDMS can also seal to itself and other flat surfaces reversibly by conformal contact (*via* van der Waals forces) [35]. Reversible bonding can be convenient, allowing the opening, cleaning and recycling of devices [36] but with the draw back that only vacuum can then be used to create pressure driven flow (this is due to the fact that the atmospheric pressure holds the device together when the pressure is lower inside the channels, whereas positive pressure inside the channels easily pushes the layers apart causing leaks).

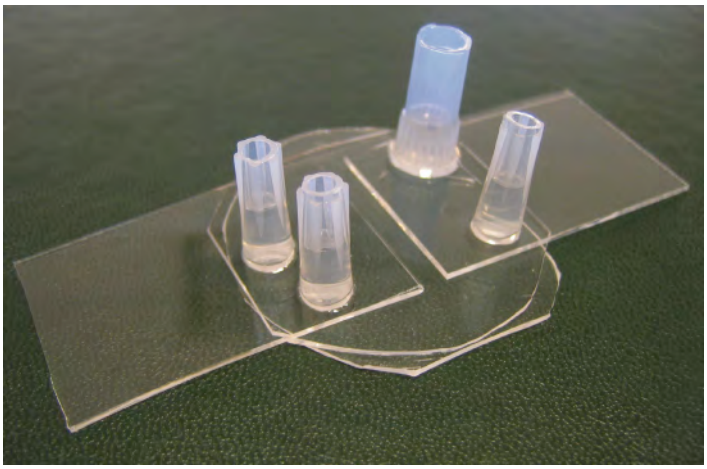

Figure 6.3 The E-DLDD ready to be placed in the stretcher chuck. *See figure 8.2.*

Quake et al [28] have reported an alternative method of achieving monolithic structures in PDMS. One layer of PDMS is mixed with an excess of one of the components (A), whereas the other layer has an excess of the other (B). After separate curing of the layers, the two layers are brought into contact. Because each layer has an excess of one of the two components, reactive molecules remain at the interface between the layers and a monolithic structure (composed of one piece of material) is achieved. The advantage of this method is that interlayer adhesion failures and thermal stress problems are completely avoided and particulates disturb interlayer adhesion much less than during plasma bonding. The disadvantage with this method is that the channels obtained are hydrophobic.

A more detailed description of the fabrication process is to be found in appendix B.

Chapter 7

Separation and Concentration

Before embarking on experiments to test the E-DLDD we wanted to see if we were able to fabricate a DLDD with a defined critical radius, in PDMS and glass. We chose to separate polystyrene beads from Duke Scientific with radii of 3.5μm from beads with radii of 5μm. The beads fluoresce at different wavelengths so it is therefore possible to identify and track them in a florescence microscope during separation.

Note: with future applications in mind, the beads where chosen for their similarity in size to red and white blood cells.

Throughout this project we have been collaborating with Martin Heller and Henrik Bruus from MIC DTU. In order to simplify the simulations that they were to perform using the same geometries as our physical devices, we first tried to make devices with a period of only three. This meant that the particles where almost as large as the gap between posts, the result being that these devices suffered from catastrophic blockages, *see figure 5.3*.

There were also problems creating a laminar flow, parallel with the channel walls due to bad positioning of the entrance and exit channels.

The next step was to simplify the design.

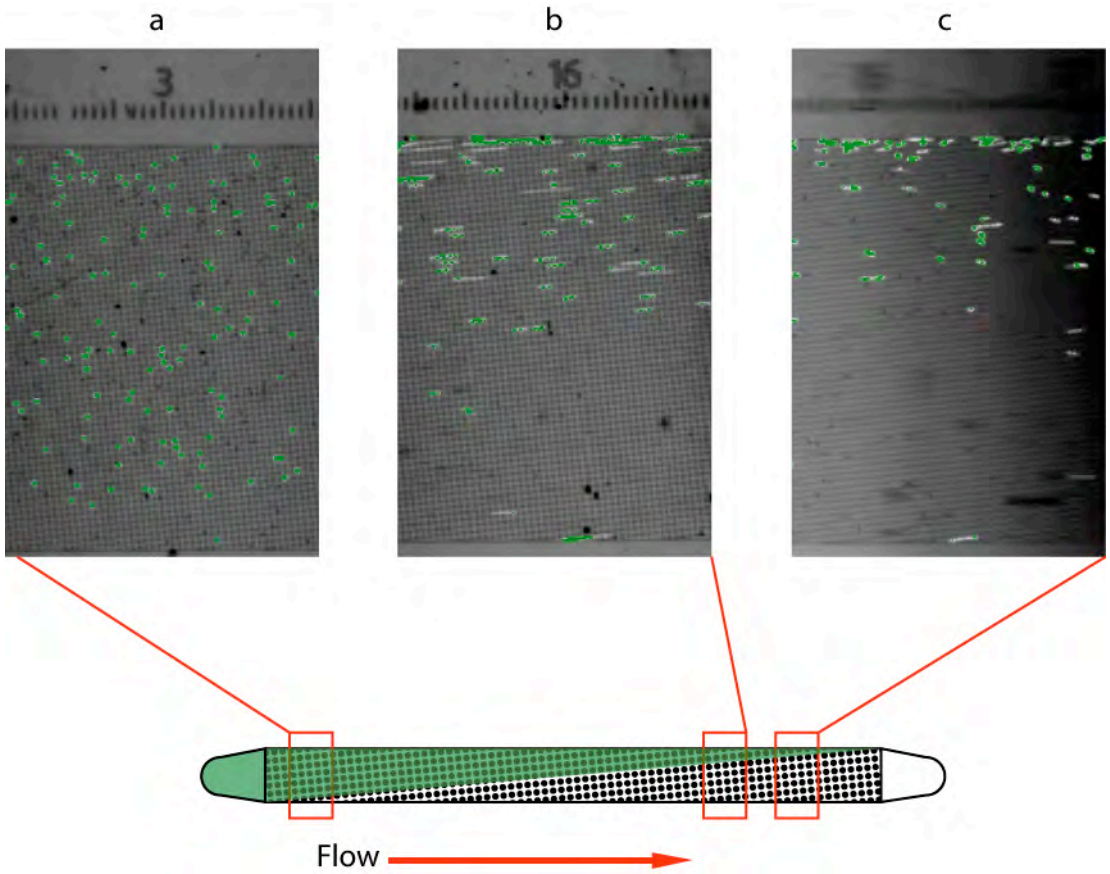

Figure 7.1 a) The beads are injected into the left-hand side of the device. The 5µm beads can be seen in green evenly distributed over the width of the device. Although not very clear in these images, the black dots are the 3.5µm beads. **b)** and **c)** The particles are displaced at $5{,}7^0$ resulting in their concentration at the top wall. It is important to note that the 7µm beads (black) are not concentrated.

7.1 Concentration

Using only one entrance and one exit (see figure 7.1) we were able to increase the concentration of the 10µm beads considerably in less than 30 seconds.

It would also be possible to concentrate these beads in a centrifuge as quickly if not quicker. The difference here is that it is only the particles that are larger than the critical size that are concentrated. The concentration is also in this case continuous. The concentrator could be integrated with other microfluidic devices in a "Lab on a Chip", something not so easily done with a centrifuge [10].

7.2 Separation

Having established that the 3.5µm and 5µm beads moved through the device with the expected angles 0° and 5.7° respectively the next step was to introduce the beads in a narrow stream in order to achieve separation. Figure 7.2 (a) shows how the device was modified in order to achieve this. The geometry of the post array was maintained but the configuration of the entrance channels was changed in order to achieve a narrow stream of particles, *see chapter 5.1.*

Figure 7.2 (b) shows the trajectories of beads through the DLDD. Although all of the 3.5μm beads moved as expected in the zigzag mode and the majority of the 5μm beads moved in displacement mode there was a tendency for some of the larger beads to move at angles less then the expected 5.7° as can be seen in the image. The standard deviation in bead sizes is, according to the manufacturers, 10%. The fact that there is no overlap of the critical size with the 3.5μm beads but that there is an overlap with the larger 5μm beads seems to indicate that the cutoff is larger than the theoretical 4.25μm.

We conclude that the geometry we have used has a cutoff somewhat larger than the theoretical 4.25μm, but without access to monodisperse beads with radii in the interval 3.5μm-5μm we were unable to determine the exact value of R_c. The device is however suitable for experiments in which d is altered and the behaviour of beads observed, which will allow an alternative method of determining R_c to that used by Huang et al [1].

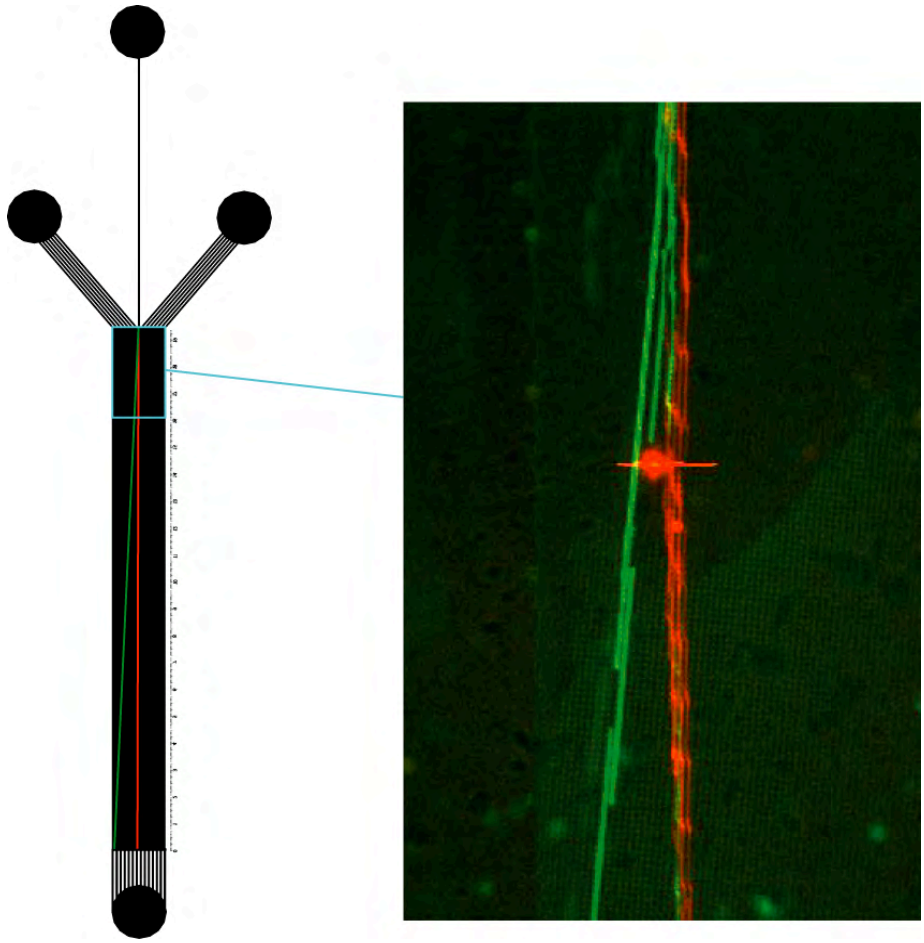

(a) (b)

Figure 7.2. (a) an illustration showing the geometry of the device used and the migration angle of the two different sized beads. Because the camera we use is black and white it is not possible to see the red and green beads simultaneously. The inset shows two micrographs taken in succession using two different wavelengths chosen to excite first one bead type and then the other. An exposure time of 1s is used in order to show the trajectories of the beads. The two images are then superimposed. The 5μm beads are seen here in green moving in displacement mode and the 3.5μm beads in red are moving in zigzag mode.

Chapter 8

Elastic properties of PDMS and the effects of stretching on device geometry

PDMS, as already mentioned, is an easily processed silicone rubber material that is very well suited to micro-fluidics applications. The elasticity of PDMS is another property that contributes greatly to its versatility and we are not the first to make use of this. Replicas cast in PDMS are easily removed from their moulds due to the elasticity of the material, making it one of the most widely used materials for soft lithography [18, 29]. As well as being used widely in microcontact printing [37] where stamps are needed that are flexible enough to conform to uneven surfaces, but also durable enough to be deformed repeatedly over long periods of time. PDMS has been used as a spring material in micromechanical sensors [38], stretched, oxidized and allowed to relax in order to create sinusoidal waves in the surface [39] and stretched, oxidized, functionalized and then allowed to relax in order to make mechanically assembled monolayers (MAMs) [40].

Although the elasticity of PDMS limits the obtainable aspect ratios of structures and channels, it also adds flexibility. Components such as pumps [28, 41] and valves [42] have been incorporated in micro-fluidics devices with great success.

We have seen how the distance between posts in the DLDD determines, for fixed N, the cutoff between the two modes of transport. By making a DLDD entirely in PDMS and mounting it in a chuck designed to stretch, it we can obtain a tuneable separation device.

Figure 8.1 The effects of global stretching on λ, both in the direction of, and perpendicular to the direction of stretching.

8.1 Young's modulus, shear modulus and Poisson's ratio of PDMS

The Young modulus, E, of PDMS ranges from $8.5 \cdot 10^5 Pa$ to $3.6 \cdot 10^5 Pa$ depending on the mixing ratio and according to [36] can be taken as 750kPa for a ratio of 10:1. The shear modulus, G, depends also on the amount of curing agent used but is approximately 250kPa for a 10:1 mixture [38].

The Poisson ratio μ can be approximated by $\mu = \frac{E}{2G} - 1$, which gives for PDMS mixed in the ratio 10:1:

$$\mu = \frac{E}{2G} - 1 = \frac{750}{2 \cdot 250} - 1 = 0.5$$

PDMS is, with the Poisson ratio of 0.5, a model rubber material.

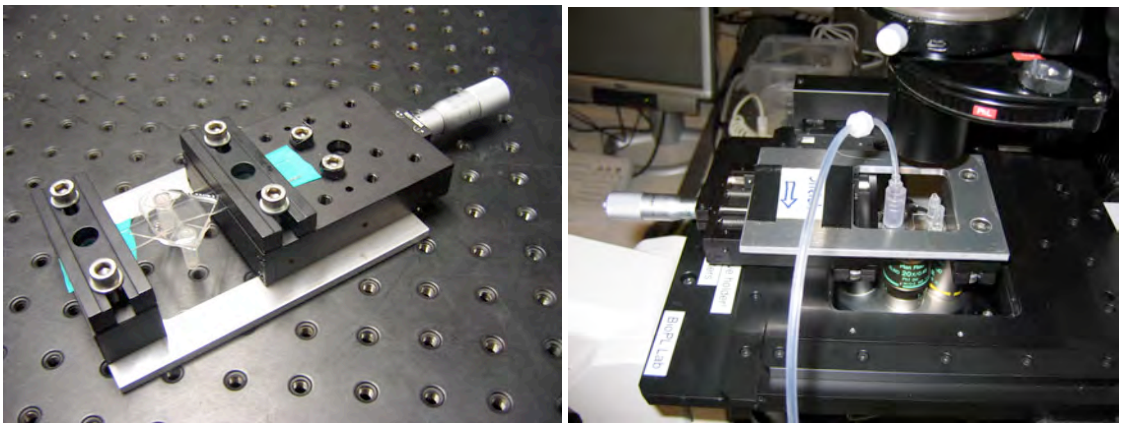

(a) **(b)**

Figure 8.2 The device is mounted in a chuck (a), essentially a modified micrometer stage for optical tables. The device can then be stretched with an accuracy of ±10μm, which over a device 10mm in width relates to a strain of 0.1%. Assuming that the percentile change is the same on all scales, i e the strain is homogeneous, this relates to being able to adjust the distance between posts originaly spaced at 10μm with an accuracy of ±10nm. (b) the chuck can be mounted in a fluorescence microscope and the device connected to pumps. It is then possible to take images of ongoing separation and to tune the cutoff in real time.

8.2 Determining the effects of stretching.

In order to stretch the DLDD in a controlled manner a chuck was adapted using a micrometer translation stage and some optical bench fittings, *figure 8.2 (a)*. The chuck is designed to be mountable in an optical fluorescence microscope *figure 8.2 (b)*. Devices held in the chuck can be connected to periphery pumps and imaged in the microscope during ongoing separation. Figure 8.3 shows the results of stretching on the distance between posts.

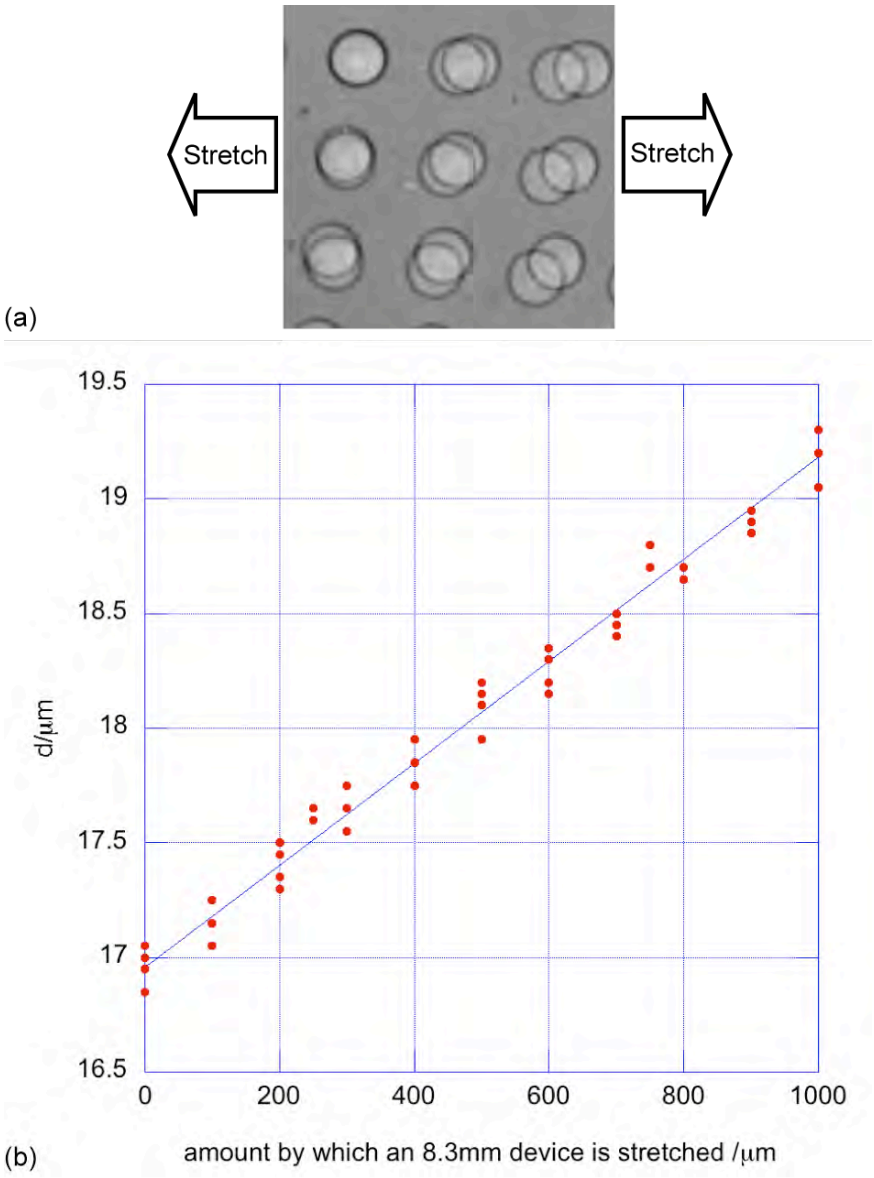

Fig. 8.3 The effects of global stretching on obstacle arrays within an E-DLDD. (a) Superposition of photographs taken before and after stretching. (b) d as a function of stretching during 15 consecutive stretching and relaxing cycles of a device 8.3mm wide. R^2=0.989

The effects of stretching on *d* were determined by repeatedly stretching the devices and then allowing them to relax. Images where analysed using Image J in order to determine *d*. Figure 8.3 shows the results of 15 consecutive stretchings of a device.

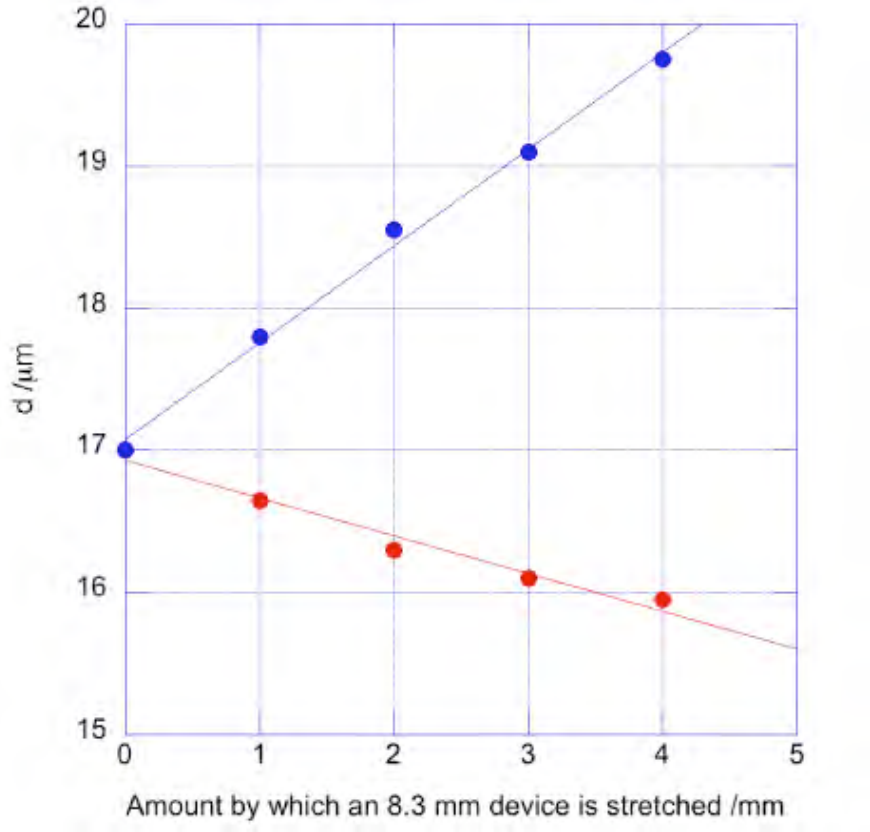

Figure 8.4 In figure 8.3 (a) one can see how the distance between obstacles, *d*, decreases perpendicular to and parallel with the direction of stretching. This effect could also be used to alter *d*.

8.3 Effects of stretching on resolution

There are several effects that will act to lower the resolution of the E-DLDD. Differences in the distances between posts will vary. Future experiments designed to determine how small this variation can be made and its effects on resolution would be of benefit.

Even if one can fabricate devices with very small variations in post separation distances, variations will be introduced due to the uneven stretching of the PDMS (or any other rubber elastic material used). It will be essential for the success of any future work to maximise the homogeneity of both the arrays and the elastomeric material used.

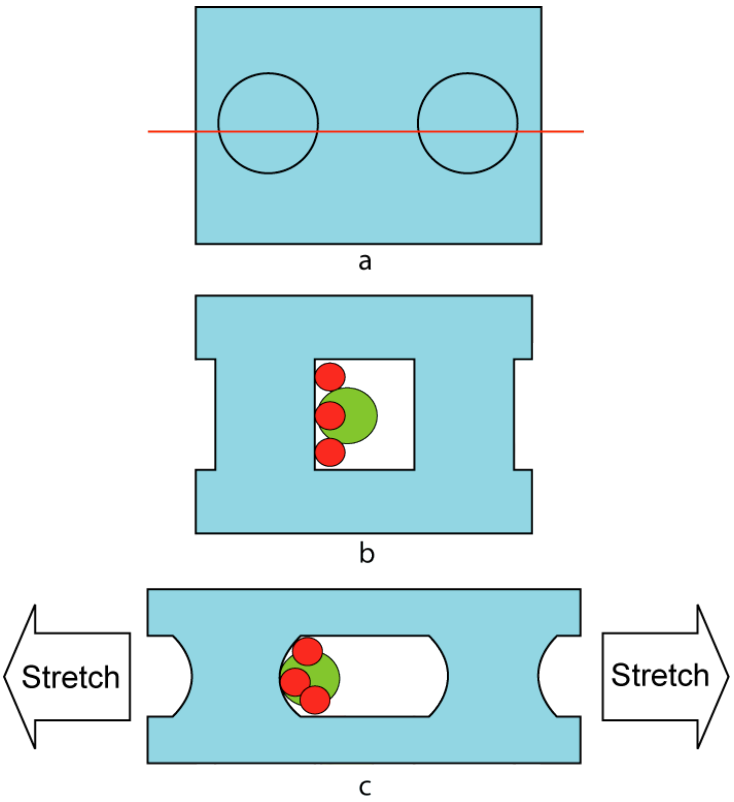

Figure 8.5 A cross section through a DLDD showing how the PDMS, in blue, is effected by stretching **(a)** The red line shows the position of the cross-section through two cylindrical obstacles in a DLDD. **(b)** In the un-stretched state the obstacle walls are straight and parallel. **(c)** Upon stretching, the shape of the cross-section changes.

The change in the cross-sectional profile of the gaps between posts is responsible for the introduction of yet another effect that could negatively affect resolution. The width of the streamlines and therefore the critical size may differ as a function of height in the channels. If particles are able to diffuse between different heights and therefore move between streams with different critical radii then the effect would lead to the broadening of zones.

8.4 Determining the uncertainty in R_c

The fit in figure 8.3 can be used to approximate the uncertainty in d as the device is stretched.

If we assume that we can decide the amount, x, by which the device is stretched, without error, then the uncertainty, σ_d, in the distance, d, between obstacles is given by:

$$\sigma_d = \sqrt{\frac{1}{N-2}\sum_{i=1}^{N}\left(d_i - A - Bx_i\right)^2}$$

where $d = A + Bx$ is the equation of the linear fit.

There is however in our case an uncertainty in x which must be combined in quadrature to the uncertainty in d. The total uncertainty $\sigma_d(tot)$ is given by:

$$\sigma_d(tot) = \sqrt{{\sigma_d}^2 + (B\sigma_x)^2}$$

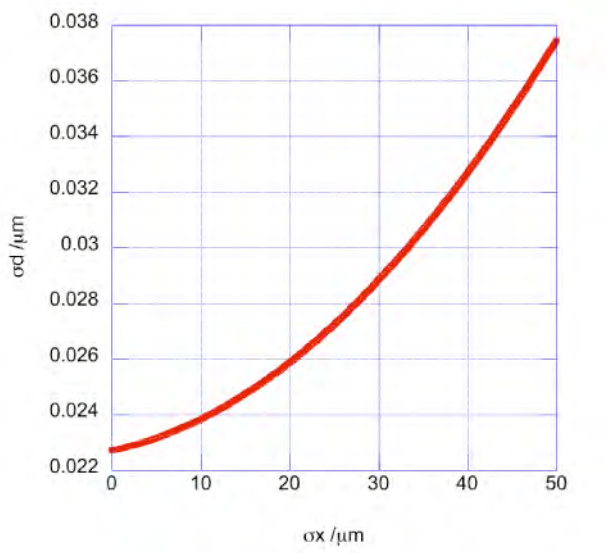

Figure 8.6 The uncertainty in R_c as a function of the uncertainty in x.

Figure 8.6 shows how the uncertainty in d depends on the uncertainty in x. We estimate the uncertainty in our stretching device to be on the order of 1μm. This gives us an uncertainty, σ_d=90nm which corresponds to an uncertainty in the cutoff size, with a period of 10, of:

$$\sigma_{R_c} = \alpha \frac{\sigma_d}{N} = 2.62 \frac{90\,nm}{10} \approx 24\,nm$$

As the slope of the curve is small in the interval [0,5μm] even a less optimistic estimate of 5μm for the uncertainty in x doesn't effect this value markedly.

8.5 Conclusion

By stretching an 8mm long PDMS device containing a DLDD with a period of 10 we can tune the cutoff size, with an uncertainty of 90nm.

There will however be other sources of error in the devices that may limit their tune ability.

The effects of stretching on the inter-obstacle distance was only determined as an average over 10 specific obstacles. There are various inhomogeneities that could lead to further uncertainties:

- Inhomogeneities in the inter-obstacle distance, d_0, before stretching would add a background uncertainty. With current processing techniques however these inhomogeneities can be made very small.
- Inhomogeneities in the elasticity of the PDMS due to imperfect mixing of the pre-polymers. These effects can be minimized by improving the mixing techniques, for example by sonicating the mixture before curing.

- Inhomogeneities in the thickness of the PDMS, which lead to inhomogeneous strain, can be minimized by improving the soft lithography process used to fabricate the devices. Moulds could be used to define thickness instead of simply pouring PDMS onto a bas-relief as we have thus far done.
- Aging
- Adsorption
- Drift
- Hysteresis

All are effects that need to be explored and quantified.

Further investigations are necessary into the limitations of elastic devices. FEM-simulations would be of value enabling us to better predict the effects of stretching. Although the homogeneity of PDMS together with fabrication issues are likely to limit the performance of E-DLDD´s, the fact that they can be tuned during separation means that some variation in the geometries of devices can be compensated for.

Chapter 9

Tunable Separation

Having tested the effects of stretching on the geometry of the post arrays, the next step was to test the effect it would have on the critical size. The effects of stretching were measured in two E-DLDD´s with the same obstacle array geometries, with theoretical R_c=4.25μm. The devices differed in the configuration of the entrance and exit channels. *Figures 9.1 and 9.3* show the two designs. Ideally the sample should be injected in a narrow

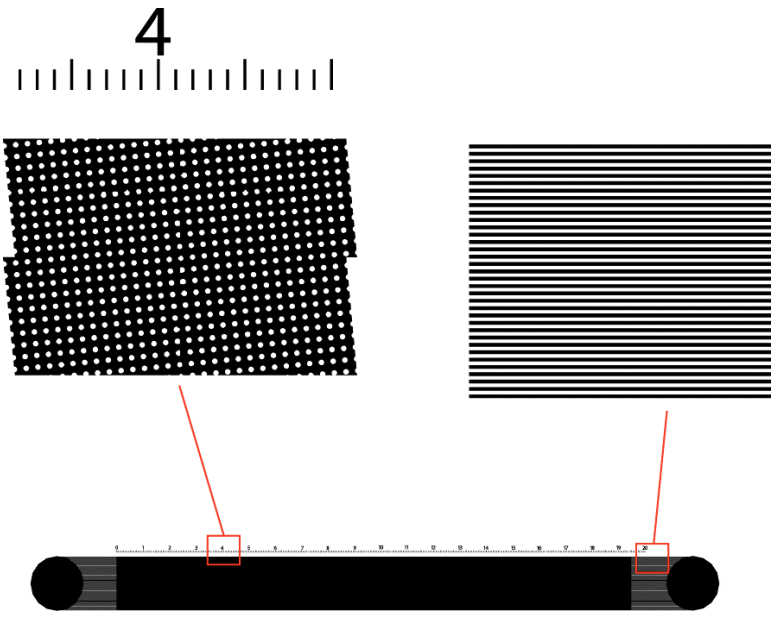

Figure 9.1 The device used for the first stretching experiment. The inset, top left, shows the post array and scale bar. The inset on the right shows the many channels used to linearise the flow profile.

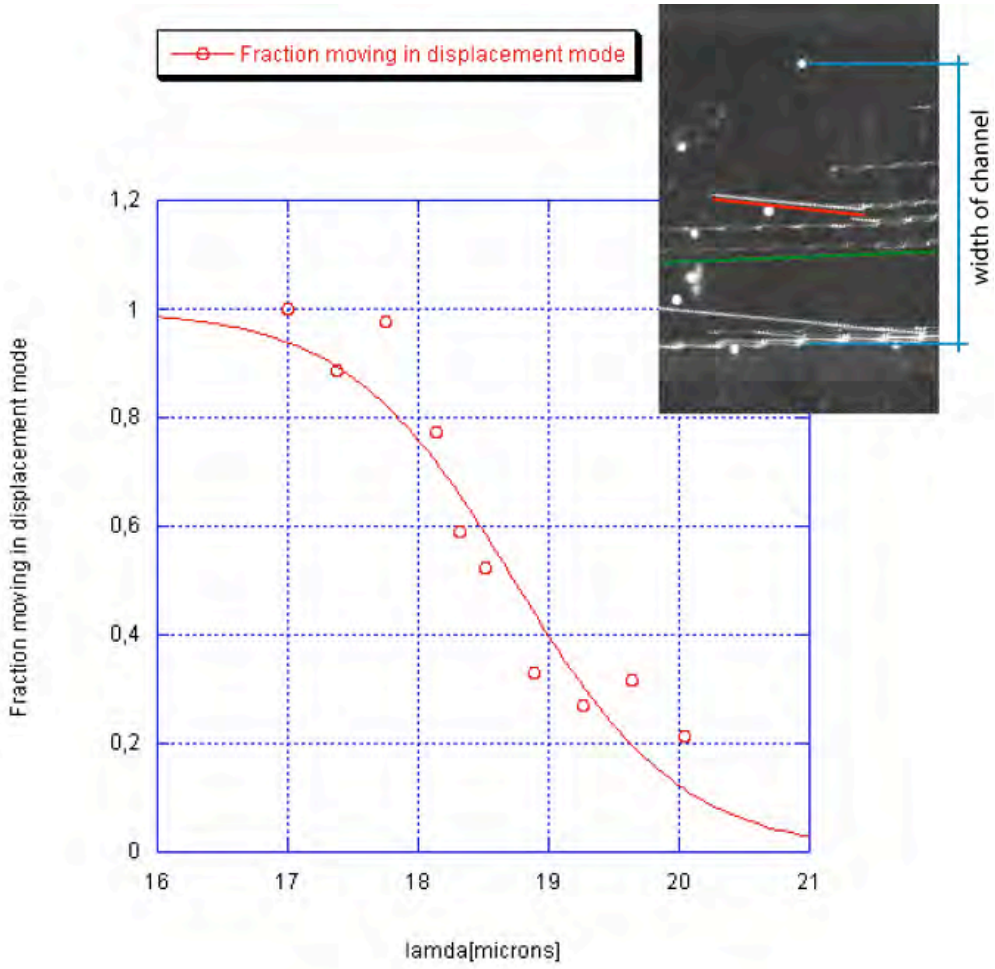

Figure 9.2 Fraction of 5µm beads moving through a DLDD in displacement mode. The original cutoff is at 8.5µm and to start with more or less all beads, being larger than the cutoff, move in displacement mode. As the device is stretched, the cutoff increases. Those beads that are smaller than the cutoff begin to move in zigzag mode. Eventually practically all beads are moving zigzag. The inset shows how the fraction of beads moving in displacement mode was established. Long exposure times were used to show the trajectories of beads. The total length of the displacement traces (red) was divided by the total length of all traces (red + green). The change in the distance between posts was established by measuring the fractional change in the width of the whole channel (blue). This fractional change was then applied to the post separation.

stream, as in the initial experiments with glass sealed devices. Initial attempts were however unsuccessful. Devices fabricated entirely in PDMS lack the support given by the glass cover. Without this mechanical support the channels often collapsed. Although this is not a fundamental problem, and can be solved simply by changing the aspect ratios of the channels, there was not room for such redesign within the timeframe of this project.

Due to the large bead sizes chosen for these initial experiments it was possible to study the behaviour of individual beads during stretching.

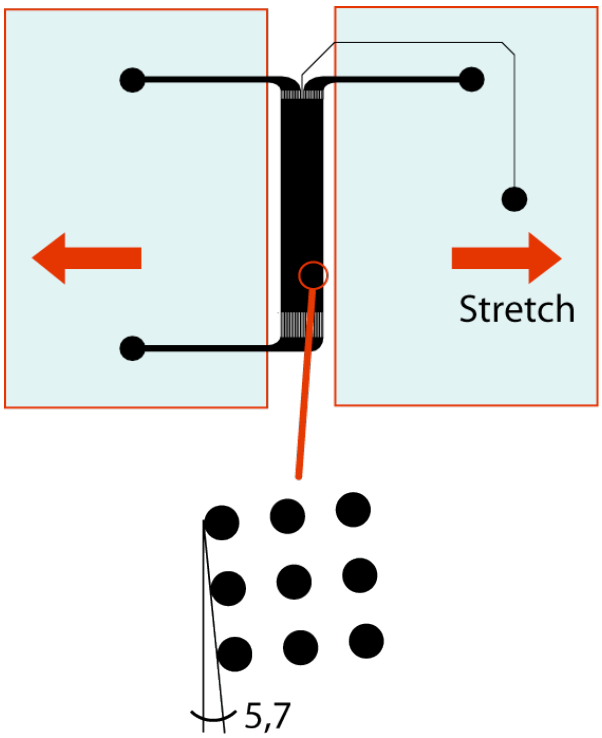

Figure 9.3 The geometry of the device used. Glass slides (blue) are bonded to the PDMS, partly to enable the bonding of reservoirs to the device and the clamping of the device in the chuck but also to define the area that is stretched; PDMS that is bonded to glass cannot stretch, and so stretching takes place only in the area between the glass slides

9.1 Effects of stretching on transport mode.

9.1.1 Experiment 1

Device 1 with a cutoff at 4.25μm was mounted in the microscope, in the stretching chuck and run with beads with 5μm radii. The device was stretched by ~20% and then allowed to relax. This procedure was repeated whilst filming continuously.

The effect on the mode of transport was immediately apparent. It was possible to switch from zigzag to displacement mode and back very easily, see figure 9.2.

The 200 frames of the film were analyzed in order to obtain the dependence of the mode of transport on the distance between posts, see inset figure 9.2.

It is evident from figure 9.2 that the transition is not abrupt. The shape of the curve reflects the distribution in the size of beads.

9.1.2 Experiment 2

In the second experiment a device with the same post geometry as experiment 1, but with entrance and exit channels as shown in figure 9.3 was used. The intention was to achieve a narrow central stream of particles and by stretching change the migration angle. Unfortunately blockages together with pumping problems, although not fundamental in nature, made the focusing of streams impossible at the time of the experiment. Laminar

flow parallel with the channel walls was however produced and it was possible to study the behaviour of beads through the devices.

Figure 9.4 shows the results of the stretching experiment. Each point in the plot shows the average migration angle of all particles in one frame of the film.

9.2 Deriving the fit function.

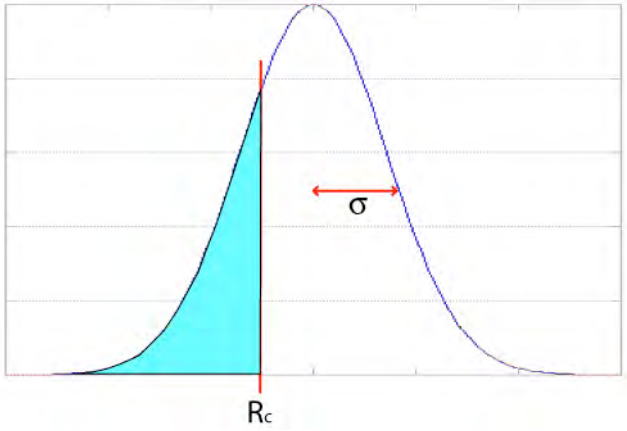

The distribution in the sizes of beads is Gaussian. If the mean size is X and the standard deviation is σ then the distribution is given by:

$$e^{-\frac{1}{2}\left(\frac{x-X}{\sigma}\right)^2}$$

When beads with a mean radius of X move through an E-DLDD the number of beads moving in either the displacement or the zigzag mode depends on R_c that in turn depends on d. As d is increased by stretching the device R_c sweeps over the distribution in sizes. The migration angle of beads in a device as a function of R_c is given by:

$$\theta = \tan\left(\frac{1}{N}\right)\left(1 - \frac{\int_{-\infty}^{R_c} e^{-\frac{1}{2}\left(\frac{x-X}{\sigma}\right)^2} dx}{\int_{-\infty}^{\infty} e^{-\frac{1}{2}\left(\frac{x-X}{\sigma}\right)^2} dx}\right)$$

This can be rewritten using the complementary error function and fitted to the data by varying the parameters X, σ and the angle of migration:

$$\frac{1}{2}\tan\left(\frac{1}{N}\right) erfc\left(\frac{x-X}{\sqrt{2}\cdot\sigma}\right)$$

Fitting this function to the data in Pro Fit using the Levenberg-Marquardt algorithm gave:

Fitted parameters	Standard deviations
Maximum angle = 5.4°	ΔMaximum angle = 0.3683°
X = 19.9896μm	ΔX = 0.3659μm
σ = 1.4611μm	Δσ = 0.4397μm

The width of the error function should reflect the width of the distribution in bead sizes plus broadening due to the device:

$$\sigma^2_{total} = \sigma^2_{beads} + \sigma^2_{device}$$

The beads have a CV of 10%, which compares well to the standard deviation of the error function, which is also 10%.

We conclude that the broadening due to the device is too small to be determined using this method.

In future projects the separation of monodispers beads in a E-DLDD would allow the broadening due to the device to be determined. These beads could themselves be obtained using a DLDD. Alternatively the behaviour of only one bead moving back and forth could be studied as *d* is altered.

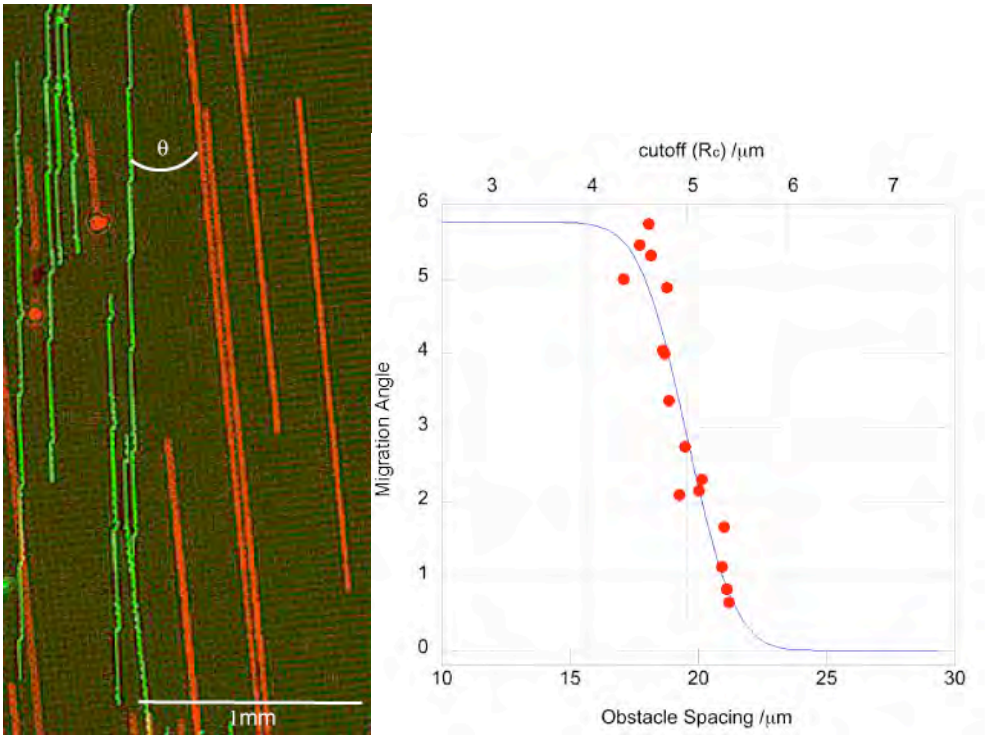

(a) (b)

Fig. 9.4 (a) Two photographs are superimposed to show how the migration paths of 5μm (radius) fluorescent beads change when the device is stretched. In red, one can see how the beads that are larger than the initial cutoff follow the geometry of the device. In green, one can see how the beads which are now smaller than the cutoff due to the subsequent stretching of the device, follow the fluid flow (fluid flow is directly down in the image). (b) The dependence of the migration angle of the polystyrene beads through the device as a function of d. 5.7° corresponds to the red particle traces in (a) and 0° to the green traces. The width of the error function reflects the Gaussian distribution in bead sizes.

9.2 Estimating the correction factor.

The error functions can be used to estimate the correction factor α. We assume that when the beads are moving half in zigzag and half in displacement mode, that is at the inflection point, the cutoff coincides with the mean size of the beads which is 5μm and we obtain:

$$\alpha = \frac{R_c N}{d} = \frac{5 \cdot 10}{20.0} = 2.5$$

which is somewhat larger than the $\sqrt{\left(\frac{N}{3}\right)}$ calculated in chapter 4.5. The actual value is expected to be larger than that calculated with the 2D model as *w* is not >>*d* as assumed in the calculation. The 3D model used by Martin Heller *(table 4.1)* is more applicable. 2.5.

Chapter 10

Applications

In this chapter we propose some applications and modifications to the DLDD in both the stretching and static modes that we have envisioned during the course of this project.

10.1 Growing Particles to Defined Sizes

A possible application of the DLDD could entail using the well defined cut off size of the device, not to sort an existing sample into spatially separated zones, but to control a process in which particles are grown by controlling the time that they spend in a reactive area. Without specifying any one particular process the general principle would be that (see figure 10.1):

- Reactants are mixed upon entering the DLDD.
- Particles move in the laminar flow, parallel with the walls, growing as they go.
- When the particles reach the size, predetermined by the geometry of the device they are pushed by the posts, out of the reactive area, whereupon they cease to grow.
- Particles can be collected and reactants, or those particles that did not reach the desired size, recycled.

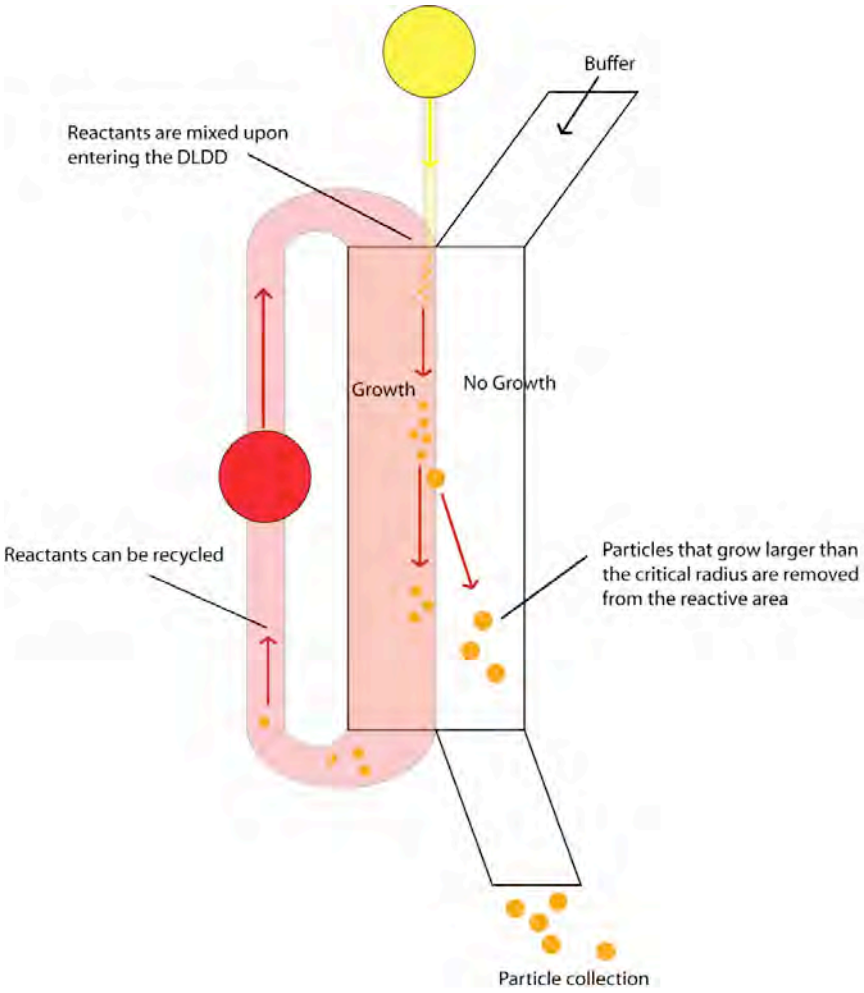

Figure 10.1. Hypothetically the DLDD could be used to define the sizes of particles that are grown by the reaction of chemical ingredients or smaller component particles. When particles reach the critical size they are displaced out of the reactive area.

If this process were carried out in an elastic device then the ability to tune the cutoff size would translate into the ability to tune the size of the particles produced.

10.2 Targeting a Specific Size in a Population of Particle Sizes: Band pass Filter

One limitation of the DLDD is the fact that it only separates those particles smaller than the critical size from those that are larger. (Particles coinciding with the critical size can move in either mode.) The serial use of two devices with a small variation, ΔR_c, in the critical sizes would enable the selection of a narrow band of beads with sizes within the range $[R_c, R_c + \Delta R_c]$ This would require the design and fabrication of many devices to achieve the isolation of many different sizes. There would also be the problem of interfacing the separate devices.

The elastic-DLDD has a variable critical size. Figure 10.2 shows how it could be possible to separate the particles by flowing them in one direction, changing the critical size by stretching and then reversing the flow. This could conceivably be automated so that the field direction and the critical size are changed many times. This would lead to the separation of particles into well defined zones in a direction perpendicular to the direction of flow.

The same effect could be obtained in a DLDD with static geometry by the careful control of the direction of particle migration via a well defined electric field, *see reference* [8]. Changing the angle, θ, between the direction of flow and the array changes the period:

$$\theta = \tan\left(\frac{1}{N}\right)$$

Which in turn changes the cutoff size.

$$R_c = \alpha \frac{d}{N}$$

Alternating the field between two angles could select particles in an interval $[R_c, R_c + \Delta R_c]$ in a similar to that described above.

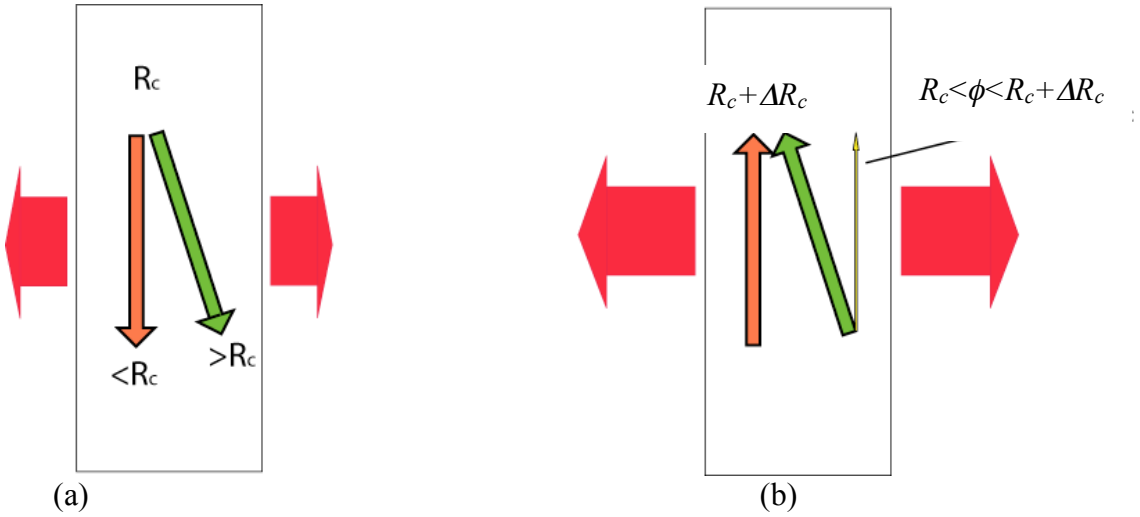

Figure 10.2 Bandpass filter. Tuneability of the cutoff size allows the selection of particles with a specific size from a population with a large spread in sizes. (a) the device is stertched to achieve a cutoff at R_c. (b) the ammount by which the the device is stretched is increased thereby increasing the cutoff to $R_c+\Delta R_c$. After reversing the flow, particles larger than $R_c+\Delta R_c$ will return along the same path (green arrow) while those in the interval $[Rc, Rc+\Delta R_c]$ will follow the direction of flow (thin yellow arrow).

10.3 Creating a Gradient of Inter-Obstacle Distances

Huang et al fabricated DLDD´s which were divided into sections with varying inter-obstacle distances (d), see figure 10.4, allowing the separation of particles into as many subsets as there are sections. With elastic devices it is possible to create a continuous gradient in d that is also tuneable. The amount by which *d* changes is dependent on the global strain, which is in turn, depends on the width of the device being stretched. By varying this distance along a device a gradient in *d* will be created upon stretching. One way to achieve this would be to vary the shape of the glass slide used to anchor the devices. Figure 10.3 (a) shows how a linear gradient could be created by varying the global deformation as a linear function of position along the device. Figure 10.3 (b) shows how other gradients could be achieved.

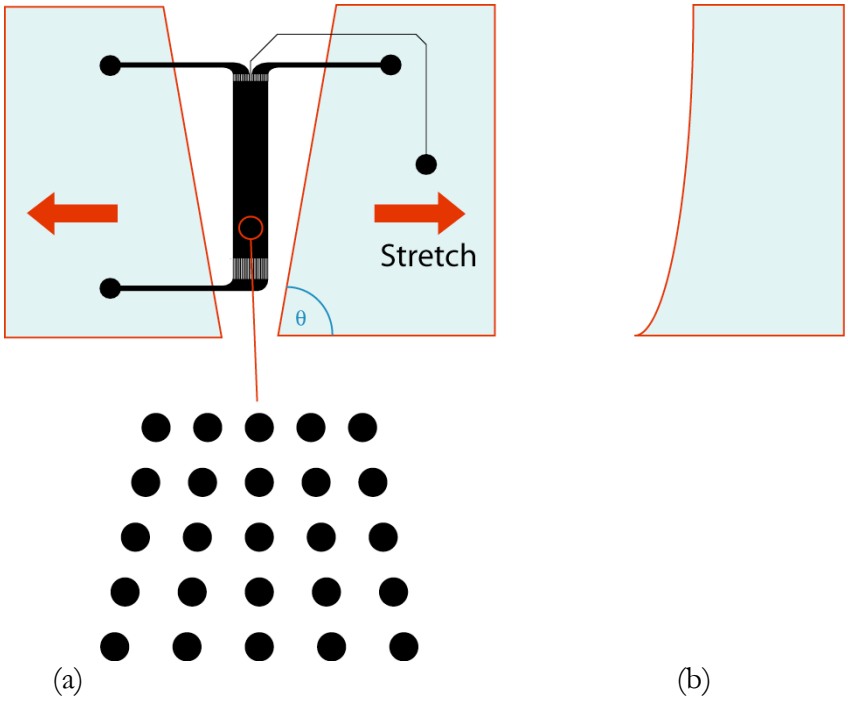

Figure 10.3 Gradients in inter-obstacle distances can be created by the inhomogeneous stretching of devices. Linear (a) or even more complicated gradients (b) could be achieved by varying the shape and positioning of the glass support that is bonded to the PDMS.

10.4 Anti Clogging Geometry

One of the problems inherent to the separation of biological samples is the large spread in the sizes of the particles present in many samples. The analysis of blood for example is hindered by the presence of blood cells. The large particles are often removed during pre-treatment. By modifying the orientation of the posts in the DLDD it could be possible to separate particles with a very large spread in sizes in one and the same device.

This design is able to achieve separation at different cutoffs, one for each post separation but due to the fact that all particles must move through each section, it is not possible to alter the inter-post distance by much. One solution would be to make the sections long enough to ensure that the particles being displaced move all the way to the edge, and then collect them.

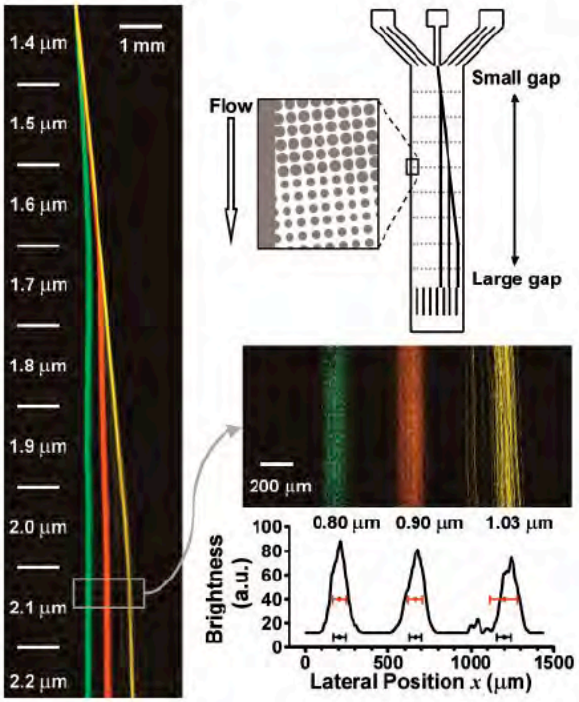

Figure 10.4. Image from L. R. Huang, *ref* [1] showing a DLDD with varying post separations.

An alternative would be to tilt the rows of obstacles as in figure 10.5. Due to the displacement of particles (to left in the figure) it would be possible to separate particles on the order of 10μm and 100nm in the same device.

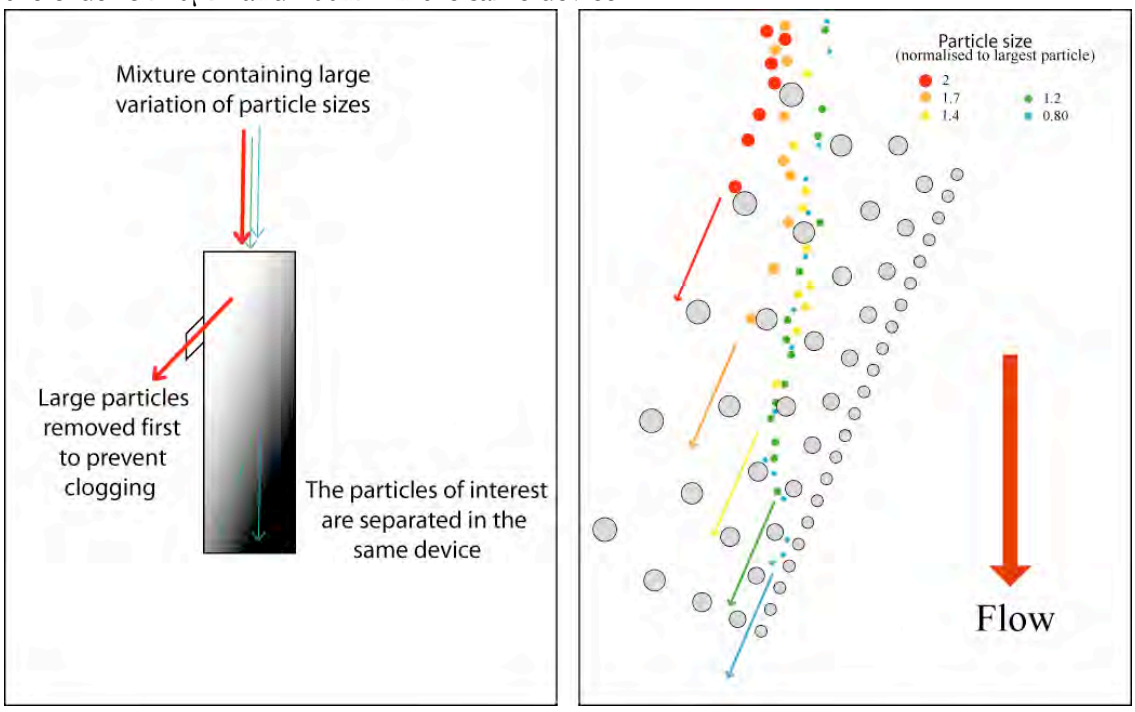

Figure 10.5 Large particles are removed to prevent clogging. Proteins could then be separated in the same array.

10.5 Morphology Based Separation

During one experiment a pair of beads that had joined together (see figure 10.6) were observed to move through the DLDD in displacement mode. The individual beads where smaller than the critical size and should therefore have moved through the device in zigzag mode. The bead pair was seen to rotate, 180^0, in travelling from one post to the next seemingly in resonance with the array.

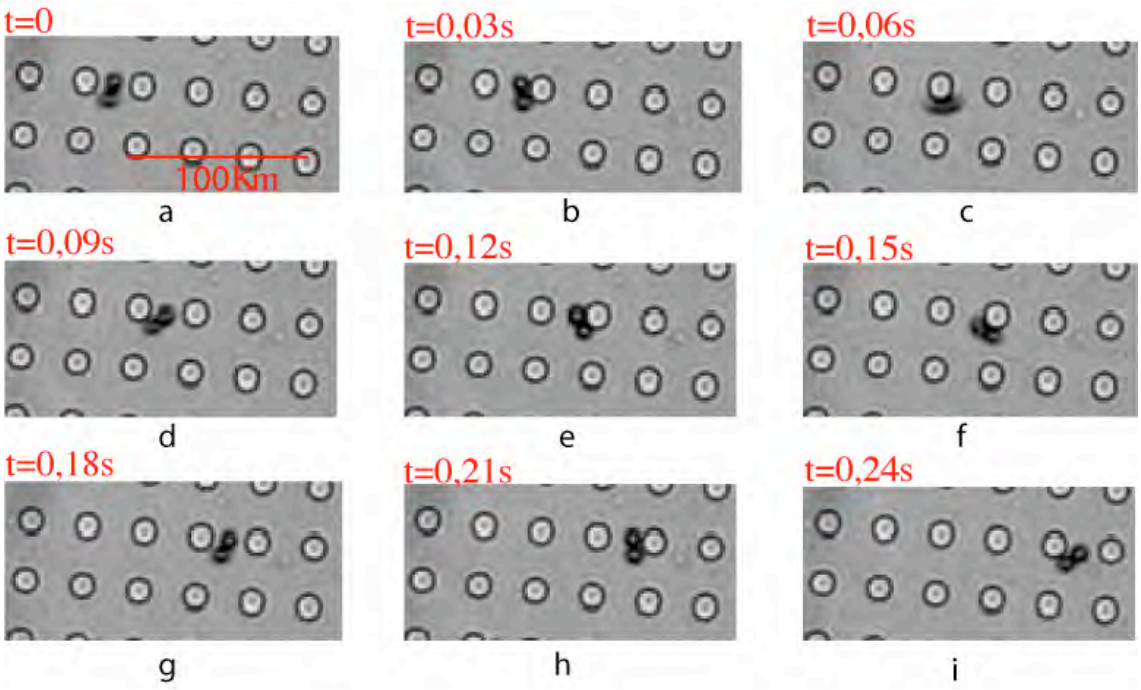

Figure 10.6. The series of images 1 to 9 show a bead pair moving through the DLDD from left to right. The pair move in displacement mode, rotating once for each post negotiated.

Occasionally particles other than those intentionally introduced appear during experiments. These particles of dust or other remnants from the fabrication process present us with an opportunity to study the behaviour of non-spherical objects in the DLDD. Figure 10.7 (a) shows a rectangular particle traversing a post array. The particle remained in this orientation for 20 or more rows, moving only in displacement mode. For some reason the particle finally rotated and was immediately able to follow the flow, zigzagging across to the adjacent row.

Figure 10.7 (c) shows a triangular particle in a DLDD. This particle was also moving in displacement mode, but this time rotating 120^0 between each of the posts encountered.

We conclude that this effect could be used to separate ridged particles with well-defined lengths or geometries, bacteria for example, by adjusting the distance between posts in order to find resonance. It may also be possible to design obstacles so that non-rigid particles are allowed to relax, or are forced into well-defined forms. The dependence on the orientation of non-symmetrical particles or the deformation of soft particles will however add a non-deterministic element to the separation. It is however of interest to pursue this line of development as there are to our knowledge at present no alternative methods of morphology based separation.

As discussed in chapter 2 both the position of the hydrodynamic centre of mass and the physical extension of the particles figure in determining the mode in which they will move. It is perhaps not realistic to assume that a large particle, in contact with several streamlines, is only effected by the one in which the hydrodynamic centre appears. The development of the DLDD stands to gain considerably from the modelling of these systems of array geometries, post shapes and particle characteristics.

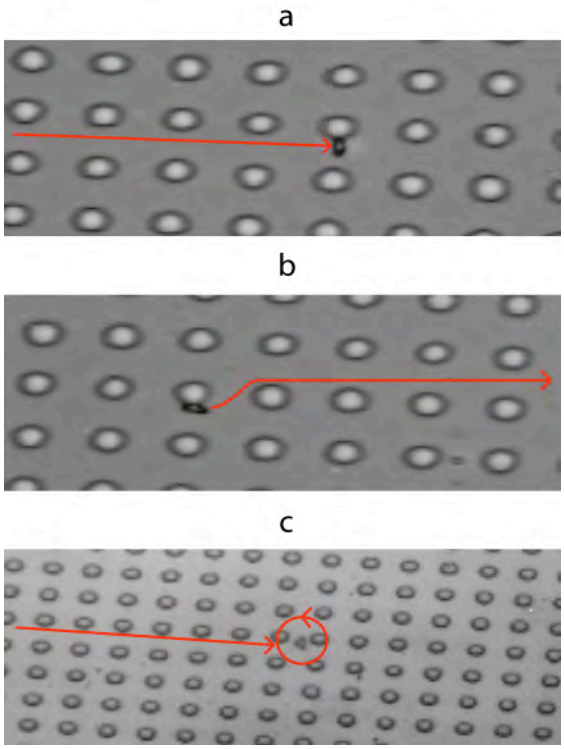

Figure 10.7 a) shows a rectangular particle presenting its longest edge to the post gap. The particle is, in this orientation, larger than the critical size and is therefore displaced laterally. **b)** After 20 rows the particle suddenly rotates and is able to fit into the streamline that goes to the left of the post (as seen from the particle's perspective). **c)** A triangular particle rotates 120^0 between each post and moves in displacement mode. The posts in all three of the images have a diameter of 17μm.

Chapter 11

Outlook

We have shown that the cutoff size in DLD devices fabricated in PDMS can be tuned during separation by controlled stretching. The behaviour of particles in DLD´s is highly dependent on their hydrodynamic radii, a property that, while easily predicted for plastic beads, can vary for biological particles depending on the conditions present. The ability to tune the cutoff during separation adds versatility to the method developed by Huang *et al* allowing not only fine adjustment, relaxing the strict fabrication requirements, but also new modes of operation for DLDD´s as discussed in chapter 10.

Although much work remains to be done in categorising the limitations of our method, FEM-simulations for example would help to predict the elastic behaviour of devices; we believe that we have shown the control of array dimensions through elastic deformation to be a viable means of achieving tuneable separation. Not only Deterministic Lateral Displacement but also many other microfluidic separation techniques, at least those dependent on device geometries, could stand to benefit from the controlled adjustment on the nanometre scale of channel dimensions or array spacings.

Appendix A

An initial attempt to determine how the resolution scales with size and period.

We define the following parameters:

L [m] = the length of the separation area in the DLDD.
t [s] = the time taken for the particles to travel the distance L.
ΔX [m] = the distance between the centres of gravity of the two zones.
$K_B = 1.381*10^{-23}$ Boltzmann´s constant.
T [K] = 300 is the temperature.
N = the period of the array.
v [ms^{-1}] = the velocity of the particles.
R_c [m] = the critical size.
η [Nsm^{-2}] = $1040*10^{-6}$ the viscosity of water.
R_s = resolution
σ [m] = Standard deviation of the Gaussian distribution of particles after traveling distance L.

The following equations can be used to investigate how the resolution scales with both the distance between posts and the period of the arrays, the two factors that determine the critical size, together with the driving pressure that determines the particle velocity and therefore the time the particles have to diffuse:

$$R_s = \frac{\Delta X}{4\sigma} \quad \text{A1}$$

$$\Delta X = \frac{L}{N} \quad \text{A2}$$

$$\sigma = \sqrt{2Dt} \quad \text{A3}$$

$$D = \frac{K_B T}{6\eta R_c \pi} \quad \text{A4}$$

$$t = \frac{L}{v} \quad \text{A5}$$

$$R_c = \frac{d}{N}\alpha \quad \text{A6}$$

$$\alpha = \sqrt{\frac{N}{3}} \quad \text{A7}$$

$$v = \frac{\Delta P d^2}{8\eta L} \qquad \text{A8}$$

$$R_s = \frac{\Delta X}{4\sigma}$$

$$= \frac{L}{N}\frac{1}{4\sqrt{2Dt}} \qquad \text{Using A2 and A3}$$

$$= \frac{L}{N}\frac{1}{4}\sqrt{\frac{6\eta R_c \pi}{2K_B T}\frac{V}{L}} \qquad \text{Using A4 and A5}$$

$$= \sqrt{\frac{6\pi}{32\sqrt{3}K_B T}}\Delta P^{\frac{1}{2}} d^{\frac{3}{2}} N^{\frac{4}{5}} \qquad \text{Using A6, A7 and A8}$$

Using vacuum pumps as we have done limits the maximum pressure to 1 atmosphere $\left(1.013\cdot 10^5 Pa\right)$, so we take this to be constant and get the following equation.

$$R_s = C \cdot d^{\frac{3}{2}} \cdot N^{\frac{4}{5}} \qquad \text{Where } C = \sqrt{\frac{6\pi\Delta P}{32\sqrt{3}K_B T}} \approx 9.1\cdot 10^9$$

Appendix B

Fabrication recipes

Master fabrication in SU-8

The following recipe is based on recommendations from Microchem, the manufacturers of SU-8. We found that some of the parameters had to be optimized in order to obtain planar surfaces during spinning, vertical profiles and good adhesion to the silicon substrate. SU-8 is available with varying amounts of solvent and hence differing viscosities that determine, together with the spin speed, the thickness of the obtained layer. The following recipe gives a 20μm layer when used with SU-8 2010.

Substrate preparation

- Ensure that the silicon substrate (2" 100 wafer) is clean and planar.
- Bake in convection oven at 200^0C for 30 minutes to remove surface water and promote the adhesion of SU-8 to the surface.

Spin coating of SU-8

- SU-8 should be applied to wafer directly upon removal from the oven in order to minimize the amount of water that can adsorb to the surface.
- Holding the wafer in one hand, and pouring from the SU-8 bottle with the other in as even a manner as possible, about one third of the wafer is covered.
- The wafer is then tilted so that the SU-8 flows over then entire surface.
- The wafer is centralized on the vacuum pad in the spinner and the following spin cycle is performed.
- 20 seconds at 500rpm-to spread the coating evenly over the wafer.
- 120 seconds at 1000rpm-to obtain 20μm layer.
- These times are longer than those recommended by Microchem but gave more even coatings of SU-8 with smaller edge beads.
- Allowing the sample to relax on a level surface for 1-2 hours can minimize edge beads.

Note: one of the greatest problems encountered was that an excess of SU-8 was needed to achieve good coverage, and this excess, when thrown off the wafer during spinning had a tendency of finding its way onto the surface. A piece of filter paper held close to the edge of the spinning wafer was used to catch this excess with good results.

Pre-Baking

Pre- and post-exposure baking was performed on a hotplate with vacuum.

- 1 min at 65^0C
- Ramp to 95^0C - takes 4-5 minutes
- 2 minutes at 95^0C
- Relax for 10 minutes on a separate hotplate at 35^0C

Exposure

- 25 seconds at 12.5 $mJcm^{-2}$.

Post exposure bake

- 1 minute at 65^0C
- Ramp to 95^0C (takes 4-5min)
- Ramp to 65^0C (by setting the hotplate to 5^0C - 8min)
- Relax 10 minutes on second hotplate at 35^0C.

Developing

- Sonicate at low amplitude (50V) for two minutes in SU-8 developer.
- The developer is rinsed away with isopropanol and the wafer dried with nitrogen.
- A white film indicates the presence of undeveloped resist, in which case further developing is required. This should be done in 1-minute steps, with intermediate rinsing, until the white film is no longer seen.

Hard Baking

- 200°C in a covection oven. This causes reflow reducing the size and number of cracks

Anti-sticking treatment of master

The silanisation process was performed using the same method and the very same equipment as that described by M. Beck in ref 29, with the exception that we found 150^0C to give the best results, namely fewer excess deposits on the surface of the master.

PDMS

Our devices where fabricated in PDMS (RTV 615 from Bayer Silicones) and sealed with either glass or a blank slab of PDMS. The devices where cast on the master (replica moulding) in the following manner.

- The PDMS is mixed with the hardener at a ratio of 9:1 by mass.
- The mixture is placed in a vacuum chamber in order to remove gas bubbles.
- The PDMS is poured onto the master.
- Bake at 80^0C for 1 hour.
- The cured PDMS is removed carefully from the master.

Glass cover

- Holes are made in the glass slides using 50μm aluminium oxide in a micro-sand blaster (Microetcher™, Danville Materials) together with a copper mask.

Reservoirs

- Reservoirs were made from pipette tips

Bonding the devices

The components are assembled in the following manner.

- The PDMS is sonicated in 99.7% ethanol for 5 minutes in order to remove uncured polymer and particles.
- The glass slide is wiped vigorously with 99% chloroform to remove any deposits left during the etching of the holes.
- Glass slide and PDMS are exposed to oxygen plasma at a pressure of 5mBar for 1 min.
- PDMS and glass (or PDMS-PDMS) are brought into contact and light pressure applied with fingertips.
- Reservoirs are attached using UV-curing glue (Norland Optical Adhesive, Norland Products, inc). The glue is applied sparingly, the reservoirs positioned and the device then exposed to UV light (320-400nm) for 10 minutes.
- Device is immediately filled with an aqueous solution (the type used depends on the application) to conserve the hydrophilicity of the channel walls.
- Devices can be stored for weeks if the reservoirs are covered in order to prevent evaporation of the liquid. Alternatively, storing the devices in a refrigerator reduces the evaporation rate considerably.

Appendix C

The Stretcher-Chuck

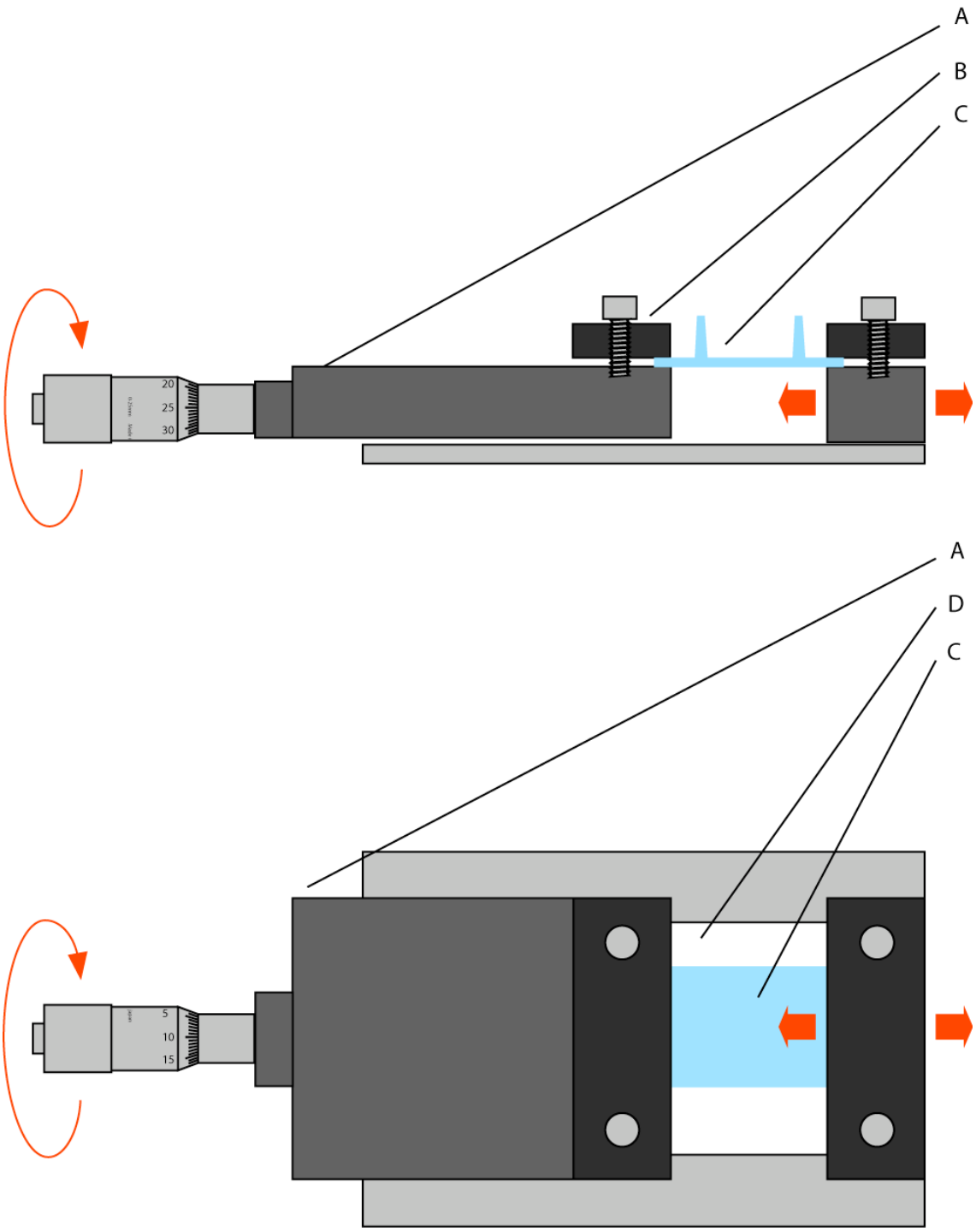

The stretcher-chuck is based on a translation stage from Mitutoyo (A). (B) Clamps were added to the translation stage to hold the devices (C) in position. The clamp on the right moves relative to the one on the left when the micrometer screw on the translation stage is adjusted. The hole (D) allows microscope access to the devices.

References

1. Lotien Richard Huang, E.C.Cox, Robert H. Austin, James C. Sturm, *Continuous Particle Separation Through Deterministic Lateral Displacement.* Science, 2004. **304**(5673): p. 987-990.
2. Malsch, I., *Protein Research Calls for Advanced Instruments.* The Industrial Physicist, 2003: p. 18-22.
3. A. Vlahou, M.F., *Proteomic approaches in the search for disease biomarkers.* Journal of Chromatography B, 2004(814): p. 11-19.
4. Sklar, J.P.N.a.L.A., *Suspension array technology: evolution of the flat-array paradigm.* TRENDS in Biotechnology, 2002. **20**(1): p. 9-12.
5. O, T.J., 2005.
6. O. Bakajin, T.A.J.D., J. O. Tegenfeldt, C. Chou, S. S. Chan, R. H. Austin and E. C. Cox, *Separation of 100-Kilobase DNA Molecules in 10 Seconds.* Anal. Chem, 2001. **73**(24): p. 6053-6056.
7. L. Richard Huang, J.O.T., Jessica J. Kraeft, James C. Sturm, Robert H. Austin and Edward C. Cox, *A DNA prism for high-speed continuous fractionation of large DNA molecules.* nature biotechnology, 2002. **20**: p. 1048-1051.
8. L. Richard Huang, J.O.T., Jessica J. Kraeft, James C. Sturm, Robert H. Austin and Edward C. Cox, *Generation of Large-area Tuneable Uniform Electric Fields in Microfluidic Arrays for Rapid DNA Separation.* IEEE, 2001.
9. Giddings, J.C., *Unified Separation Science*. 1991: John Wiley & Sons, Inc.
10. www.gyros.com
11. Kim, J.; Jang, S. H.; Jia, G.; Zoval, J. V.; Da Silva N. A. and Marc J. Madou. *Cell Lysis On a Microfluidic CD (Compact Disc)*. Lab On a Chip 4 (5): 516-522 , 2004.
12. http://scienceworld.wolfram.com/physics/Navier-StokesEquations.html.
13. M. Heller, H.B., *Particle motion in mirofluidics simulated using a Femlab implementation of the level set method.* unpublished, 2005.
14. Heller, M., *Dynamics of finite sized particles in microfluidic systems*. 2005.
15. David J. Beebe, G.A.M., Glenn M. Walker, *Physics and Applications of Microfluidics in Biology.* Annu. Rev. Biomed. Eng, 2002. **4**: p. 261-286.
16. Niels Asger Mortensen, F.O., Henrik Bruus, *Reexamination of Hagen-Poiseuille flow: shape-dependence of the hydraulic resistance in microchannels.* Phys. Rev. E, 2005. **71**.
17. C R Tamanaha, L.J.W.a.R.J.C., *Hybrid macro–micro fluidics system for a chip-based biosensor.* J. Micromech. Microeng, 2002. **12**: p. N7-N17.
18. Whitesides, J.C.M.a.G.M., *Poly(dimethylsiloxane) as a material for fabricating microfluid devices.* Accounts of Chemical Research, 2002. **35**(7): p. 491-499.
19. B. Bilenberg, M.H., D. Johansen, V. ¨Ozkapici, C. Jeppesen, P. Szabo, I. M. Obieta, O. Arroyo, J. O. Tegenfeldt and A. Kristensen, *Topas Based Lab-on-a-chip Microsystems Fabricated by Thermal Nanoimprint Lithography.* unpublished, 2005.

20. C. Duffy, J.C.M., O. J. A. Schueller, G. M.Whitesides, *Rapid Prototyping of Microfluidic Systems in Poly(dimethylsiloxane).* Anal. Chem, 1998. **70**(23): p. 4974-4984.
21. S. Zheng, R.Y., Y.-C. Tai and H. Kasdan, *Deterministic Lateral Displacement Mems Device for Continuous Blood Cell Separation.* unpublished.
22. Weigl BH, B.R., Cabrera CR, *Lab-on-a-chip for drug development.* Advanced Drug Delivery Reviews, 2003. **55**(3): p. 349-377.
23. Liu R, S.M., Sharp K, Olsen M, Santiago J, et al, *Passive mixing in a three-dimensional serpentine microchannel.* J. Microelectromech. Syst., 2000. **9**: p. 190-97.
24. Jacobson S, M.T., Ramsey J., *Microfluidic devices for electrokinetically driven parallel and serial mixing.* Anal. Chem, 1999. **71**: p. 4455-59.
25. Abraham D. Stroock, S.K.W.D., Armand Ajdari, Igor Mezic, Howard A. Stone, George M. Whitesides, *Chaotic Mixer for Microchannels.* Science, 2002. **295**: p. 647-651.
26. Wolfgang Fraunhofer, G.W., *The use of asymetrical flow field-flow fractionation in pharmaceutics and biopharmaceutics.* European Journal of Pharmaceutics and Biopharmaceutics, 2004. **58**: p. 369-383.
27. Ning-Ping Huang, R.M., Janos Voros, Marcus Textor, Rolf Hofer, Antonella Rossi, Donald L. Elbert, Jeffrey A. Hubbell, and Nicholas D. Spencer, *Poly(L-lysine)-g-poly(ethylene glycol) Layers on Metal Oxide Surfaces: Surface-Analytical Characterization and Resistance to Serum and Fibrinogen Adsorption.* Langmuir, 2001(17): p. 489-498.
28. Unger MA, C.H., Thorsen T, Scherer A, Quake SR., *Monolithic Microfabricated Valves and Pumps by Multilayer Soft Lithography.* Science, 2000. **288**(5463): p. 113-117.
29. Whitesides, S.K.S.G.M., *Microfluidic devices fabricated in poly(dimethylsiloxane) for biological studies.* Electrophoresis, 2003. **24**: p. 3563-3576.
30. H Lorenz, M.D., N Fahrni, N LaBianca¶, P Renaud and P Vettiger§, *SU-8: a low-cost negative resist for MEMS.* J. Micromech. Microeng, 1997. **7**: p. 121-124.
31. M. Beck, M.G., I. Maximov, E.-L. Sarwe, T.G.I. Ling, M. Keil, L. Montelius, *Improving stamps for 10 nm level wafer scale nanoimprint lithography.* Microelectronic Engineering, 2002. **61–62**: p. 441–448.
32. Renée A. Lawton, C.R.P., Anne F. Runge, Walter J. Doherty III, S. Scott Saavedra, *Air plasma treatment of submicron thick PDMS polymer films: effect of oxidation time and storage conditions.* Colloids and Surfaces A: Physicochem. Eng. Aspects, 2005. **253**: p. 213-215.
33. Kenis, P.J.A.I., Rustem F.; Whitesides, George M., *Microfabrication Inside Capillaries Using Multiphase Laminar Flow Patterning.* Science, 1999. **285**(5424): p. 83-86.
34. D. C. Duffy, O.J.A.S., S. T. Brittain, G. M.Whitesides, J. Micromech., Microeng, 1999. **9**(211).
35. J. C. Lötters, W.O., P. H. Veltink, P. Bergveld, *Polydimethylsiloxane, a photocurable rubberelastic polymer used as a spring material in micromechanical sensors.* Microsystem Technologies, 1997: p. 64-67.
36. Deniz Armani, C.L.a.N.A., *Re-configurable fluid circuits by PDMS elastomer micromachining.* IEEE, 1999: p. 222-227.
37. B. Michel, A.B., A. Bietsch, E. Delamarche, M. Geissler, D. Juncker, H. Kind, J.-P. Renault, H. Rothuizen, H. Schmid, P. Schmidt-Winkel, R. Stutz and H.

Wolf, *Printing meets lithography: Soft approaches to high-resolution patterning.* IBM. J. Res & Dev., 2001. **41**(5): p. 697-719.
38. J C Lötters, W.O., P H Veltink and P Bergveld, *The mechanical properties of the rubber elastic polymer polydimethylsiloxane for sensor applications.* J.Micromech. Microeng., 1997. **7**: p. 145-147.
39. Xingyu Jiang, S.T., Xiangping Qian, Emanuele Ostuni, Hongkai Wu, Ned Bowden, Philip LeDuc, Donald E. Ingber, and George M. Whitesides, *Controlling Mammalian Cell Spreading and Cytoskeletal Arrangement with Conveniently Fabricated Continuous Wavy Features on Poly(dimethylsiloxane).* 2002. **18**: p. 3273-3280.
40. Jan Genzer, D.A.F.a.K.E., *Fabricating Two-Dimensional Molecular Gradients via Asymetric Deformation of Uniformly-Coated Elastomer Sheets.* Adv. Mater, 2003. **15**(18): p. 1545-1547.
41. Burton, B.B.a.Z., *Adhesion and friction properties of polymers in microfluidic devices.* Nanotechnology, 2005. **16**: p. 467-478.
42. Rustem F. Ismagilov, D.R., Paul J. A. Kenis, Daniel T. Chiu, Wendy Zhang, Howard A. Stone and George M. Whitesides., *Pressure-Driven Laminar Flowin Tangential Microchannels: an Elastomeric Microfluidic Switch.* Anal Chem, 2001. **73**(19): p. 4682-4687.
43. James B. Knight, Ashvin Vishwanath, James P. Brody, and Robert H. Austin, *Hydrodynamic Focusing on a Silicon Chip: Mixing Nanoliters in Microseconds.* Physical Review Letters, 1998. **80**(17): p. 3863-3866
44. N Darnton, O Bakajin, R Huang, B North, J O Tegenfeldt, E C Cox, J Sturm and R H Austin., *Hydrodynamics in 21/2 dimensions: making jets in a plane.* J. Phys.:condens. Matter, 2001. **13**: p. 4891-4902